OVERLAP PARAMETERS OF D_2-D_2 MOLECULAR PAIRS FROM COLLISION-INDUCED INFRARED ABSORPTION

RAYMOND JOSEPH PENNEY

OVERLAP PARAMETERS OF D_2-D_2 MOLECULAR PAIRS FROM COLLISION-INDUCED INFRARED ABSORPTION

by

© R.J. Penney, B.Sc.

A thesis submitted in partial fulfillment
of the requirements for the degree of
Master of Science

Department of Physics
Memorial University of Newfoundland

April 1980

St. John's Newfoundland

Canada

ABSTRACT

The collision-induced absorption of the fundamental band of D_2 in the pure gas at 77, 196, and 298 K was recorded for a number of gas densities up to 60 amagat with two 2 m absorption cells. Binary and ternary absorption coefficients of the band have been derived from the measured integrated absorption coefficients. An analysis of the absorption profiles has been performed by assuming appropriate line shapes, and the characteristic half-width parameters δ_d and δ_c of the short-range overlap-induced transitions and δ_q of the long-range quadrupole-induced transitions have been derived. This analysis also made it possible to separate the contributions of these two types of transitions to the total intensity of the band. For the D_2-D_2 collision pairs, the overlap parameters λ and ρ, which represent the magnitude and range, respectively, of the induced dipole moment, and $\mu_{overlap}(\sigma)$, the overlap-induced dipole moment at the Lennard-Jones intermolecular diameter have been determined. These parameters are compared with those of H_2-H_2 and HD-HD, reported earlier from this laboratory [S.P. Reddy, G. Varghese, and R.D.G. Prasad, Phys. Rev. A 15, 975 (1975); S.P. Reddy and R.D.G. Prasad, J. Chem. Phys. 66, 5259 (1977)].

ACKNOWLEDGEMENTS

I wish to thank Professor S.P. Reddy for suggesting the research project described here and for helping me in the preparation of the thesis.

I also extend my sincere thanks to Dr. R.D.G. Prasad for his help throughout the progress of the work.

My thanks are also due to Dr. N.H. Rich, who originally designed the 2.1 m monel absorption cell, for useful discussions in connection with the operation of the cell.

I wish to thank Professor C.W. Cho, Head, Department of Physics, for his personal interest and for his permission to pursue this research project on a part time basis.

I also thank the technical staff of the Physics Department for their advice and for their cooperation in preparing various parts for the experimental set-up.

Finally, the author appreciates the use of computer facilities provided by Memorial University of Newfoundland.

CONTENTS

CHAPTER 1

INTRODUCTION

Symmetric diatomic molecules such as H_2 and D_2 have no electric dipole moments in their electronic ground states and as a result they do not possess allowed infrared spectra. However, these molecules give rise to collision-induced infrared spectra because of the electric dipole moments induced in them by intermolecular interactions which are operative during binary or higher order collisions. In the collision process, the induced dipole moment is modulated by the rotation and vibration of the molecules and by their relative translational motion. The molecules thus absorb energy from the source of radiation by the interaction of the induced dipole moment with the radiation field, in the spectral regions corresponding to vibration-rotation, pure rotation, and translation.

Since the discovery of the phenomenon of collision-induced infrared absorption in compressed O_2 and N_2 by Crawford, Welsh, and Locke (1949), a great amount of work has been done by various researchers on the collision-induced infrared absorption of H_2. A detailed review of the work done on this aspect of H_2 until 1971 is given by Welsh (1972). For the subsequent work on H_2 the reader is

referred to Reddy et al. (1977a), Sen et al. (1980), and Reddy et al. (1980), and the references therein. A considerable amount of work on the collision-induced absorption of the fundamental band of HD has been done in the last few years, mostly in our laboratory, and for this work the reader is referred to Reddy and Prasad (1977b) and the references therein.

The collision-induced fundamental band of D_2 in the pure gas has been studied for gas pressures up to 250 atm at room temperature by Reddy and Cho (1965) and for low pressures at temperatures in the range 24-77 K by Watanabe and Welsh (1965). The band has also been studied in binary mixtures of D_2-He, D_2-Ar, and D_2-N_2 at room temperature by Pai et al. (1966) and in D_2-He and D_2-Ne at different temperatures by Russell et al. (1974). The collision-induced 1st overtone band of gaseous D_2 has been investigated in the pure D_2 gas and in D_2-Ar and D_2-N_2 mixtures at room temperature by Reddy and Kuo (1971). For references on the investigation of the collision-induced absorption of solid D_2 and of D_2 dissolved in liquids of argon, neon, and nitrogen the reader is directed to Russell et al. (1974).

According to the theory of collision-induced absorption (Van Kranendonk, 1957, 1958), the electric dipole moment (μ_{ind}) induced in a pair of colliding molecules is represented by the so-called exponential - 4 model and the interaction potential is expressed by the Lennard-Jones

intermolecular potential. In this model, the induced dipole moment is represented as the sum of two additive moments: a short-range isotropic overlap moment with $\mu_{overlap} \propto \exp(-R)$ and a long-range angle-dependent (quadrupole-induced) moment with $\mu_{quad} \propto R^{-4}$, where R is the intermolecular separation between the colliding pair of molecules. The quantity $\mu_{overlap}$ which arises due to the distortion of the electron charge distribution of the colliding pair gives rise mainly to the broad $Q_{overlap}$ ($\Delta J=0$) transitions, and μ_{quad}, which results from the polarization of one molecule by the quadrupole field of the other molecule, gives rise to relatively less broad O ($\Delta J=-2$), Q_{quad} ($\Delta J\neq 0$), and S ($\Delta J=+2$) transitions, J being the rotational quantum number. The subscripts 0 and 1 attached to O, Q, and S throughout this thesis refer to the change in the vibrational quantum number v, i.e., 0 for pure rotational transitions, 1 for fundamental transitions, etc.

One common feature of the Q branch of the collision-induced fundamental bands of H_2 and its isotopes is the occurrence of the dips in the $Q_{overlap}(J)$ components. The low- and high-wavenumber sides of these dips are designated as Q_P and Q_R, respectively. The separation between Q_P and Q_R is very much density-dependent at a given temperature. Van Kranendonk (1968) has shown that the dip in the Q branch can be interpreted in terms of the negative correlations existing between the short-range overlap dipole moments ($\mu_{overlap}$) in <u>successive</u> collisions between

molecules. The other common feature of the collision-induced infrared spectra is the occurrence of double transitions in which both molecules of the collision pair simultaneously absorb a single quantum of radiation. These double transitions are of special significance when both partners of collision are diatomic. In the quadrupolar induction-mechanism the isotropic part of polarizability of the colliding molecules contributes to the intensity of the single transitions $O_1(J)$, $Q_1(J)$ $(J\neq 0)$, and $S_1(J)$, and double transitions of the forms $Q_1(J) + Q_0(J)$ ($J\neq 0$ for the orientational transition) and $Q_1(J) + S_0(J)$. On the other hand, the anisotropic component of the polarizability contributes to the relatively weak double transitions of the type $S_1(0) + S_0(J)$ (see for example, Sen et al., 1980); in the present work we are not concerned with these transitions.

In the collision-induced fundamental band of normal D_2 at 77 K all possible transitions arising from the overlap and quadrupolar (with isotropic polarizability) induction mechanisms are shown in Fig. 1. At 77 K almost all the molecules are distributed among the rotational levels $J = 0$, 1 and 2 of the ground vibrational state. The energy levels in Fig. 1 were calculated from the constants of the free D_2 molecule (McKellar and Oka, 1978) and the transitions are shown in the following four groups: (i) $O_1(2)$, (ii) $Q_1(J)$ which includes $Q_{1\ \mathrm{overlap}}(J)$ and $Q_{1\ \mathrm{quad}}(J)$ $(J\neq 0)$;

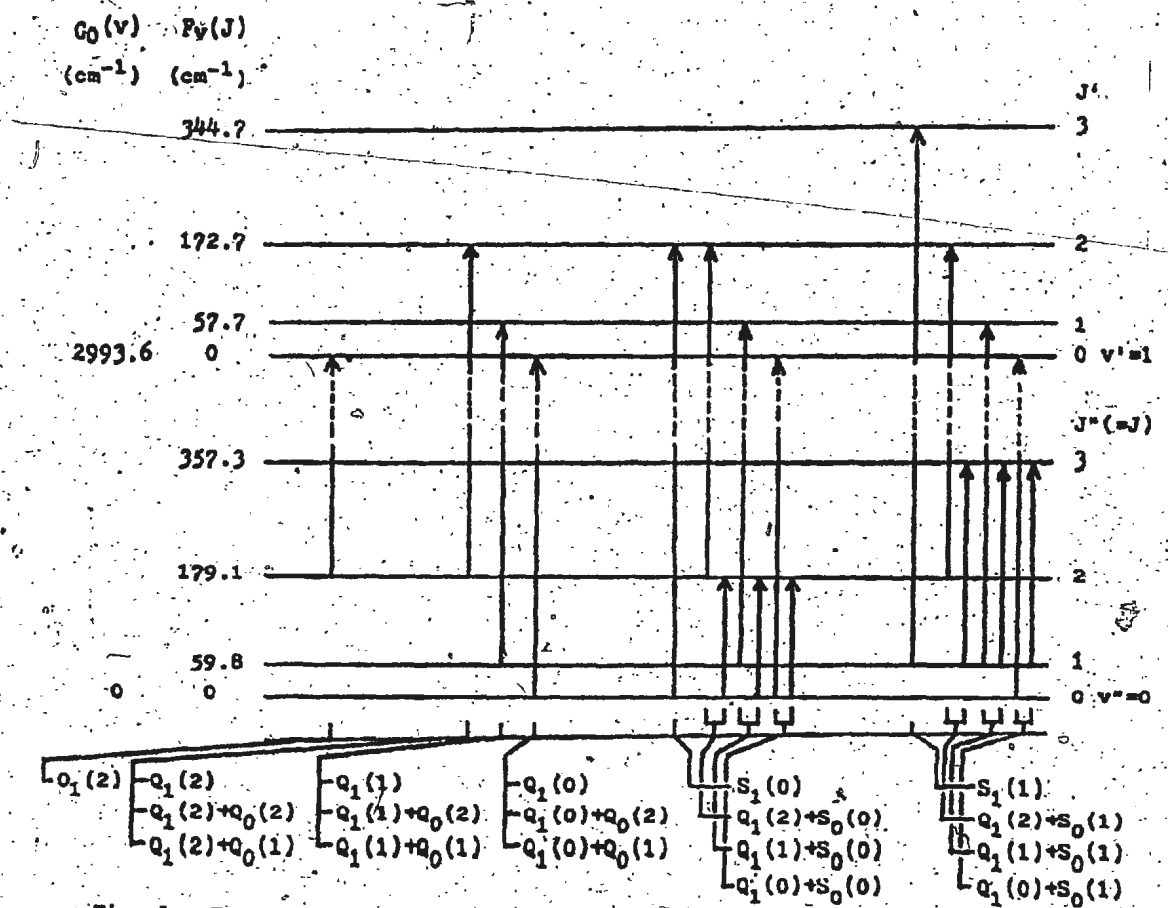

Fig. 1. Energy level diagram showing transitions arising from the overlap and quadrupolar induction mechanisms in the collision-induced fundamental band of normal D_2 at 77 K (see text for details).

$Q_1(J) + Q_0(J)$ ($J \neq 0$ in the second molecule), (iii) $S_1(0)$ and $Q_1(J) + S_0(0)$, and (iv) $S_1(1)$ and $Q_1(J) + S_0(1)$. In this figure the wavenumbers of the transitions increase from the left to the right.

Prior to the present work, no attempt was made to carry out a systematic analysis of the profiles of the collision-induced absorption spectra of D_2. However, great progress has been made in the analysis of the collision-induced absorption spectra of H_2 (see, for example, Reddy et al. 1977a; Sen et al., 1980; and Reddy et al., 1980) and of HD (see, for example, Reddy and Prasad, 1977b). The salient features of the analyses of the collision-induced fundamental bands of these molecules can be briefly summarized as follows: The intracollisional part of the $Q_{overlap}$ components arising from single collisions has been represented by the so-called Levine-Birnbaum line shape (Levine and Birnbaum, 1967) in the form of a modified Bessel function of the second kind and the intercollisional dip of these components arising from negative correlations in successive collisions (Van Kranendonk, 1968; Lewis, 1976, and the references therein) has been represented by a dispersion-type line shape. The quadrupolar components have been expressed in the form of an empirical dispersion-type function (Kiss and Welsh, 1959). The relative intensities of the quadrupolar components have been calculated from the theoretical matrix elements of the quadrupole moment and

polarizability of H_2 and HD given by Birnbaum and Poll (1969), Poll (1971), and Poll and Wolniewicz (1978). (For more details see Chapter 4).

The aim of the present research project was to make a systematic study of the collision-induced fundamental band of D_2 in the pure gas for a number of gas densities at temperatures 77, 196, and 298 K, first by obtaining accurate experimental profiles and then by carrying out profile analysis by assuming line shapes which have been used successfully in the analysis of the collision-induced infrared spectra of H_2 and HD in our laboratory and elsewhere. Details of the experimental techniques are given in Chapter 2. The experimental absorption profiles and the derived absorption coefficients of the band are presented in Chapter 3. The method of profile analysis and the results obtained therefrom are given in Chapter 4. Finally, the overlap parameters which characterize the induced overlap dipole moment in D_2-D_2 collision pairs are determined in Chapter 5.

CHAPTER 2

EXPERIMENTAL TECHNIQUES

The research project on the collision-induced absorption of the infrared fundamental band of molecular deuterium was carried out at three temperatures, 77, 196, and 298 K. A 2 m low-temperature high pressure absorption cell for work at 77 and 196 K, a 2.1 m absorption cell (originally designed for use at temperatures in the range 77-298 K) for work at room temperature, an infrared recording spectrometer and a high-pressure gas handling system were used in obtaining the experimental data. A brief description of the experimental set-up and details of the technique will be presented in this chapter.

2.1. The 2 m Stainless Steel Absorption Cell

The 2 m absorption cell is of the transmission type and was originally designed for experiments at room temperature by Reddy and Kuo (1971). With additional design and modification it was used at low temperatures down to 77 K by Chang (1974), Prasad (1976), and Sen (1978) (See Sec. 2.3(a)).

The absorption cell was constructed from a 2 m stainless steel rod 7.62 cm in diameter with a central bore 2.54 cm through its entire length. A polished stainless

steel light guide with an aperture 1.0 cm x 0.5 cm was fitted inside the central bore from one end to the other to facilitate good transmission of radiation from source to the spectrometer and to reduce the volume of the experimental gas under investigation. It was constructed in five sections to ease the problem of handling and placement.

The transmission windows at the ends of the absorption cell are synthetic sapphire discs 1.00 cm thick and 2.54 cm in diameter. Each of these windows was cemented to a stainless steel window seat having an aperture of 1.02 cm x 0.51 cm. A pressure-tight seal between the window seat and the body of the cell was achieved by using an invar O-ring between them and by tightening a retaining end piece against the body of the cell with eight Allen-head bolts.

Frosting of cell windows at low temperatures was prevented by providing each end of the cell with a vacuum housing 10 cm long and 10.5 cm in diameter which consisted of a stainless steel tube and an adapter made from Delrin material. The stainless steel section of the housing was sealed to the cell body with an indium seal. The Delrin adapter was sealed to the stainless steel section with a neoprene O-ring. A sapphire window 5.08 cm in diameter and 0.30 cm thick was appropriately sealed to the adapter by means of a rubber O-ring. The vacuum housings were continuously evacuated during experiments at low temperature. The cell was supported on discs in a double walled stainless steel jacket. The space between the walls of the

jacket was insulated with vermiculite. An opening in the top of the jacket provided easy access for the coolants. The coolants used were liquid nitrogen (77 K) and dry ice-acetone mixture (196 K).

A high pressure gas handling system [section 2.3(d)] was connected to the center of the cell by means of a 1.27 cm Aminco fitting. A more detailed description of the cell is given by Prasad (1976).

2.2. The 2.1 m Monel Absorption Cell

The 2.1 m transmission-type monel absorption cell was originally designed for experiments at any temperature between liquid nitrogen and room temperatures. It was also intended for use with chemically active gases such as hydrogen halides.

A schematic diagram of a cross-section of the cell is given in Fig. 2. It was made from a monel tube 2.1 m long, 7.62 cm in outer diameter and 2.54 cm in wall thickness. A polished monel light guide with an aperture 1.00 cm x 0.50 cm was inserted into the cell. A heating coil was wound around the cell body. Welded around the cell are two concentric steel jackets. The space between the inner jacket and the cell constitutes a heat-exchange chamber which can be filled with a gas such as helium at one atmosphere or less. The space between the two jackets is used as a liquid nitrogen chamber. Sapphire windows 2.54 cm in diameter and 1.00 cm thick were attached to the

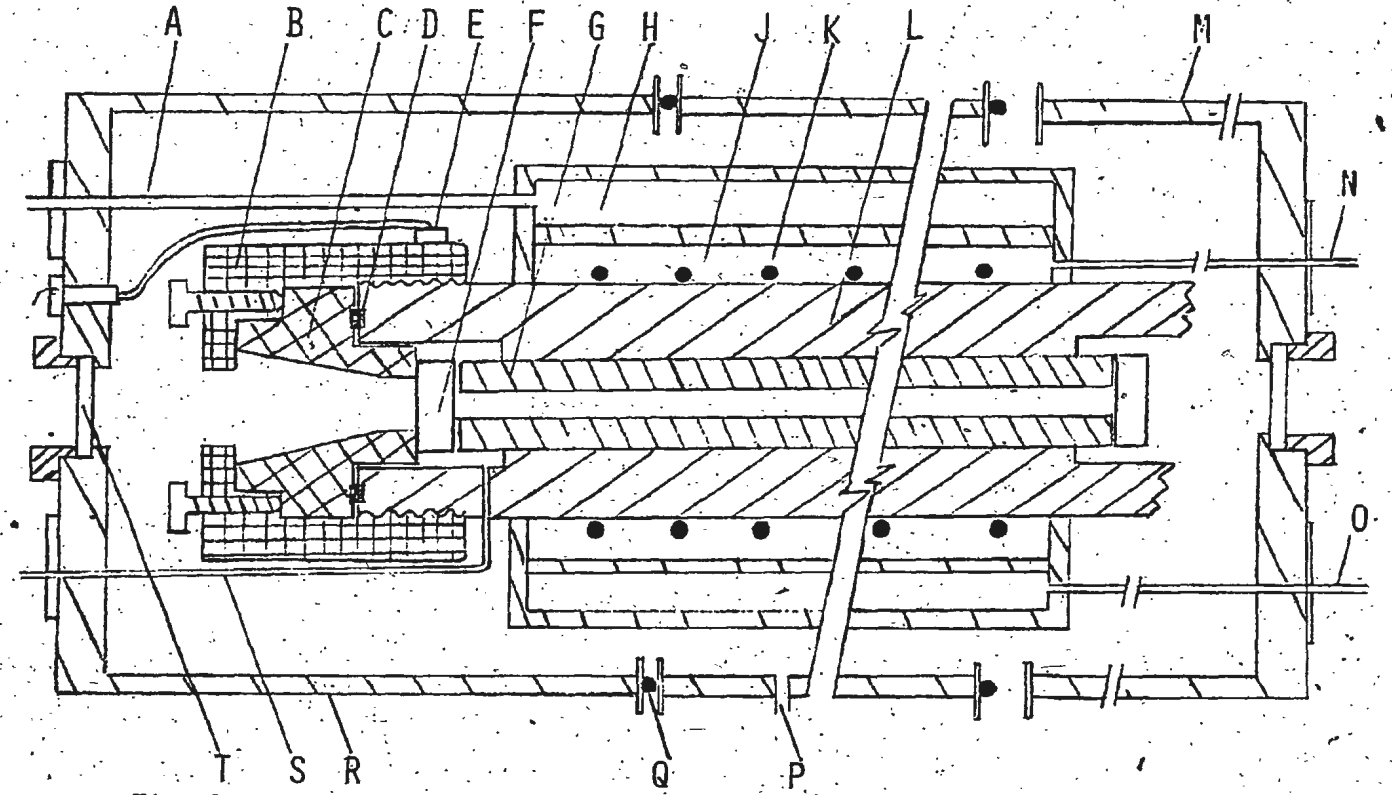

Fig. 2 A cross-sectional view of the 2.1 m monel absorption cell:

A-liquid N_2 outlet
B-window clamp
C-window holder
D-invar pressure seal
E-thermocouple and leads
F-sapphire window
G-light guide
H-liquid N_2 chamber
J-heat exchange chamber
K-heating coil
L-body of the cell
M-vacuum end cap
N-gas exchange chamber input
O-liquid N_2 inlet
P-evacuation port
Q-rubber O-ring seal
R-vacuum end cap
S-experimental gas inlet
T-outer sapphire window

polished monel window seats of the cell by means of General Electric RTV-108 clear silicone rubber cement. The outer jacket was wrapped with an aluminum coated mylar sheet and was held inside an evacuable aluminum jacket by means of nylon supports. The end caps of the aluminum jacket were fitted with sapphire windows 5.08 cm in diameter and 0.30 cm thick. The mylar wrapping and the vacuum space surrounding the liquid nitrogen chamber helped to reduce the rate of consumption of liquid nitrogen considerably. The heat exchange chamber allows the indirect cooling of the cell. In principle, the temperature of the cell can be maintained at any desired value between 77 K and room temperature by warming the cell body by passing sufficient current in the heating coil. It can be monitored with a thermistor mounted in the cell body in its mid-section and with a copper-constantan thermocouple mounted on the window clamp assembly.

In the present research project, the monel cell was successfully used for the experiments at room temperature. Several experiments at low temperatures were also performed with this cell. However, it was later realized that the thermistor in the body of the cell gave unreliable readings and the readings of the thermocouple near the window of the cell did not give the actual temperature of the gas inside the cell. Because of this difficulty the experiments at 77 and 196 K were repeated with the less cumbersome 2 m stainless steel absorption cell described in

section 2.1 and completed successfully.

2.3. The Experimental Set-Up

(a) The Source of Radiation, Optical System and the Infrared Monochromator

A schematic arrangment of the source of continuous infrared radiation, the focusing optics at both ends of the 2 m stainless steel absorption cell and the infrared monochromator is shown in Fig. 3(a). The source is a globar (silicon carbide rod) held in a water-cooled metal housing and was operated at a constant temperature of ~ 1500 K with operating voltage supplied by source radiation controller model 10, supplied by Warner and Swasey Co., Flushing, N.Y. Radiation from the source was focused on the entrance window of the absorption cell by a front-coated concave mirror M_1 (r = 60 cm and f. number = 4). After it passed through the exit window of the cell, it was focused on the entrance slit of the monochromator by a mirror M_2 which is identical to M_1. The monochromator is a Perkin-Elmer model 99 single-beam double-pass instrument, modified to its present form by the author from a basic Perkin-Elmer model 98 single-beam single-pass instrument by removing the baffles and mounting the mirror flats M_5-M_7. It was equipped with a lithium fluoride prism P. A lead sulphide detector mounted in a glass dewar and supplied by Infrared Industries, Waltham, Mass., was installed in a mount attached to the monochromator. The optical path of a

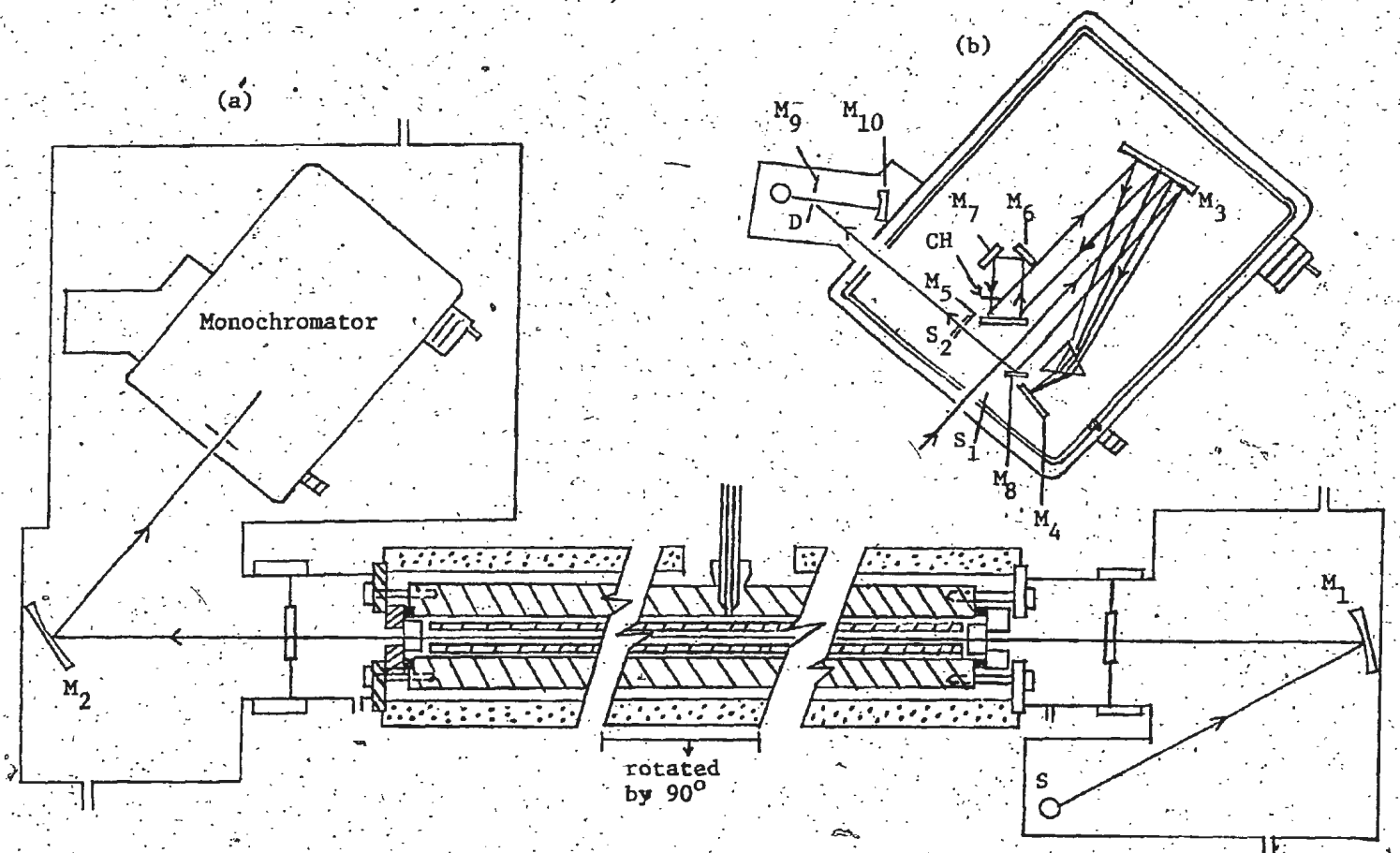

Fig. 3. (a) A cross-sectional view of the 2 m absorption cell and the optical arrangement: S, source; M_1 & M_2, spherical mirrors. (This cell was described in Sec. 2.1).

(b) Path of the monochromatic radiation inside the monochromator; S_1 & S_2, entrance and exit slits; M_3, a 21° off-axis parabolic mirror; M_4, littrow mirror; $M_5 - M_9$, plane mirrors; M_{10}, parabolic mirror; CH, tuning fork chopper; D, dewar mounted PbS detector.

monochromatic beam inside the monochromator is also shown in Fig. 3(b). Radiation after the first pass through the prism and reflection from the littrow mirror M_4 was brought to a focus between the plane mirror M_6 and model L-40 tuning fork chopper CH (American Time Products, New York, N.Y.) by the off-axis paraboloid mirror M_3. The diverging beam from the focus was chopped by the chopper and was further dispersed by the prism and finally brought to a focus on the exit slit of the monochromator. Radiation was then brought to a final focus on the detector with the help of a plane mirror M_9 with an exit hole 0.5 cm diameter and a concave mirror M_{10}.

Different wavelengths of the spectrum were brought to the detector by rotation of the littrow mirror M_4 which was coupled to a wavenumber drum driven by a three speed motor. The slit-width was maintained at 65 μm which gave a spectral resolution of ~ 2.0 cm^{-1} at 2994 cm^{-1}, the origin of the fundamental band of D_2.

(b) Signal Detection

Radiation signal which was chopped at a frequency of 260 Hz by the tuning fork chopper was focused on the dewar-mounted lead sulphide detector, cooled with liquid nitrogen [Fig. 3(b)]. This photo-conductive detector was used with a 0.1 MΩ load resistor and a 45 V battery bias supply. The output signal from the detector was a.c. coupled to a model 261 preamplifier and then to a model 131

lock-in voltmeter. Both instruments were supplied by Brower Laboratories, Waltham, Mass. The lock-in voltmeter was operated at 260 Hz which was selected with a plug-in frequency card. Within the lock-in voltmeter the amplified signal was fed to a synchronous rectifier which was locked to a square-wave reference signal from the tuning fork chopper. Phasing controls on the voltmeter permitted peaking for correct phase and thus for maximum signal. The 0-10 volt output of the lock-in voltmeter was fed to a decade attenuator G.R. model 1450 TB which has a range of 111 db attenuation in steps of 0.1 db, thus permitting a very selective operation range of outputs. The varying d.c. output from the lock-in voltmeter was finally fed to a H.P. model 7132 A strip chart recorder which was operated at a chart speed of 5.08 cm per minute.

(c) Nitrogen Flushing

The spectral region around 2.8 μm of the fundamental band of deuterium has considerable atmospheric water vapor absorption. It was therefore found necessary to remove water vapor from the entire optical path from the source to the detector. To achieve this, two air-tight plexiglas boxes, one at each end of the absorption cell, were built over steel frames mounted on steel base plates. Plexiglas sheet 0.64 cm thick was bolted to the frames and sealed with G.E. RTV silicone rubber cement. The source of radiation and focusing mirror (M_1) were housed in the box at the entrance

end of the absorption cell, and the monochromator and the other focusing mirror (M_2) were housed in the box at the exit end of the cell. These boxes were connected to the absorption cell with rubber tubes and hose clamps. A Delrin tube was fitted over the dewar containing the PbS detector and through the plexiglas top of the exit box. It was provided with air-tight seals at both places. This arrangement provided an access for filling the dewar with liquid nitrogen, which does not interfere with the atmosphere of the exit box. Two neoprene gloves were fitted to the two opposite sides of the exit box so that the monochromator settings could be handled without breaking the air-tight seal. The boxes were continuously flushed with dry nitrogen gas which was generated by boiling off liquid nitrogen contained in a 200 liter dewar by electrical heating through a 100 ohm-20 watt resistor immersed in it. The voltage across the resistor was adjusted to regulate the flow of nitrogen into the boxes. By continuous flushing of nitrogen for several days, absorption due to atmospheric water vapor was brought to a negligible and steady state.

(d) Gas Handling

A schematic arrangement of the gas-handling system is shown in Fig. 4. The absorption cell was connected to a C.P. grade deuterium cylinder supplied by Matheson of Canada, Whitby, Ontario, by stainless steel Aminco fittings through a liquid nitrogen trap made of copper coil 0.64 cm in outer diameter. Three Bourdon tube

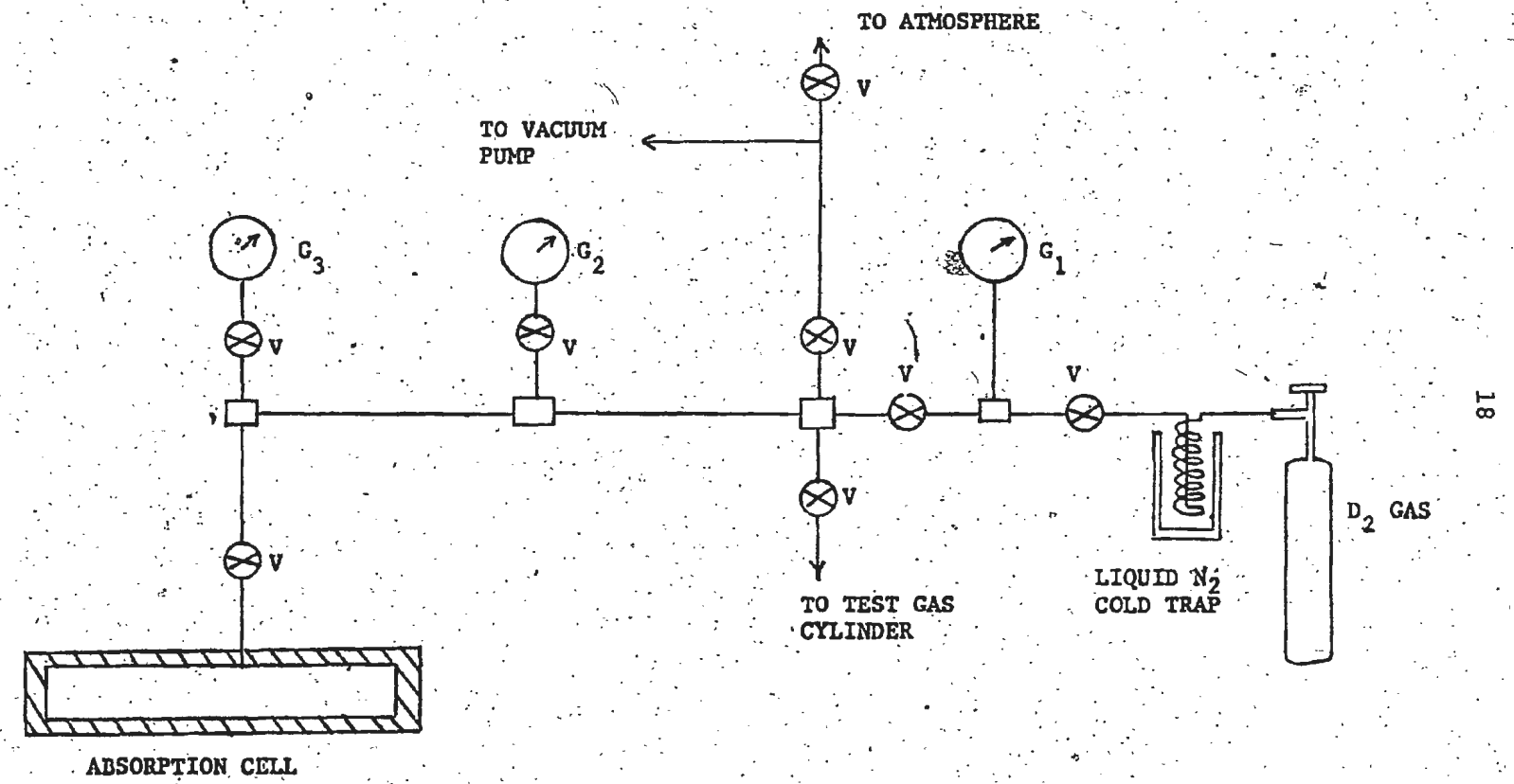

Fig. 4. The gas-handling system.

pressure-gauges G_1, G_2, and G_3, having ranges up to 500, 1000, and 5000 p.s.i., respectively, were calibrated against standard oil pressure gauges which were in turn calibrated against an Ashcroft dead-weight pressure-balance. Aminco needle valves were used throughout the high pressure system. The cold trap in the system was used for purification of the deuterium. The gas-handling system was initially tested for good vacuum and for pressures greater than those used in the actual deuterium experiments.

2.4. Calibration of the Spectral Region

Absorption lines of atmospheric water vapor (IUPAC Tables of Wavenumbers 1977), HCN, CH_4, HCl, and HBr (Rao et al., 1966) were used as standards for calibration of the spectral region 2500-4000 cm^{-1}. The distances of the absorption lines were accurately measured from the water absorption line at 3904.2 cm^{-1}. A least squares polynomial fit of the distance against wavenumbers of the standard absorption lines was made with an IBM 370 computer. A polynomial of order 5 was found to be most satisfactory. The coefficients of the polynomial obtained from the best fit were used for drawing a calibration chart at intervals of 5 cm^{-1} in the region 2500-3800 cm^{-1} with a PDP 1140 computer. Two absorption peaks occurring at 3650 cm^{-1} and 3566 cm^{-1} were used as references on the calibration chart.

2.5. Reduction of Data from the Strip Chart Recordings

If $I_0(\nu)$ is the intensity of radiation at a wavenumber ν transmitted by an evacuated cell of sample path length ℓ and $I(\nu)$ is the corresponding quantity with the cell filled with deuterium at a given density ρ_{D_2}, the absorption coefficient $\alpha(\nu)$ is defined by the relation

$$I(\nu) = I_0 \exp [-\alpha(\nu)\ell], \qquad (1\text{-a})$$

or

$$\alpha(\nu) = (1/\ell) \ln [I_0(\nu)/I(\nu)]. \qquad (1\text{-b})$$

It is to be noted that both $I_0(\nu)$ and $I(\nu)$ are measured with reference to the zero (infinite absorption) line on the chart recordings. During an experiment transmission profiles giving $I_0(\nu)$ were first recorded. These are the background recordings. Profiles were then taken for various densities of the gas in the cell. These are the $I(\nu)$ profiles. Transmission profiles of $I(\nu)$ were transferred to one of the background recordings. The quantity $\log_{10} [I_0(\nu)/I(\nu)]$ was measured at intervals of 5 or 10 cm^{-1} with the help of the wavenumber calibration chart and a standard logarithmic scale. Absorption profiles were then obtained by plotting $\log_{10} [I_0(\nu)/I(\nu)]$ against ν. The integrated absorption coefficient of the band, i.e., $\int_{band} \alpha(\nu) d\nu$ was derived from the area under the absorption profiles.

Hydrogen and deuterium are strictly symmetric molecules and hence possess ortho and para modifications. Unlike H_2, for reasons of nuclear statistics and symmetric and antisymmetric nature of rotational levels, ortho-D_2 molecules exist in even rotational levels ($J = 0, 2, 4, \ldots$) and para-D_2 molecules exist in odd rotational levels ($J = 1, 3, 5, \ldots$). It turns out that the ratio of the concentrations is 2:1 in normal deuterium. In the experiments at 77 K the possibility of conversion of para to ortho modification in the stainless steel cell was checked on the basis of the following experimental evidence: the absorption of the $S_1(0)$ line of D_2 at a given density of the gas at 77 K was monitored over a period of 12 hours and no change in absorption was observed.

2.6. Isothermal Data for Deuterium

It is convenient to express the density of a gas in the unit of amagat which is the ratio of the density of the gas at any temperature and pressure to its density at STP. Since Loschmidt's number n_0 is the number of molecules per cm^3 at STP, the product of the density of the gas at any temperature and pressure, expressed in amagat, and n_0 gives directly the number of molecules per cm^3 at the same temperature and pressure.

The pressure-density data of deuterium at 298 K and 196 K were obtained from Michels and Goudeket (1941) and Michels *et al.* (1959), respectively. There are no

similar data available in the published literature for deuterium at 77 K. However Woolley, Scott, and Brickwedde (1948) have outlined a procedure of obtaining the pressure-density data for deuterium at any temperature from the data of hydrogen at the same temperature. Using this procedure Sinha (1967) in his unpublished thesis has evaluated pressure-density data for deuterium at 77 K for densities up to 600 amagat. In the present work, these data were used.

CHAPTER 3

ABSORPTION PROFILES AND ABSORPTION COEFFICIENTS

A summary of the previous work on the collision-induced infrared absorption of D_2 and of the objectives of the present research project have been given in Chapter 1. Experimental details and the methods of obtaining absorption profiles of the fundamental band D_2 have been described in Chapter 2. The band was studied in the pure gas at 77, 196, and 298 K with 2 m and 2.1 m absorption cells and absorption profiles were obtained for several densities up to 60 amagat. Table I summarizes the experimental conditions under which the experiments were carried out.

TABLE I. Summary of the experimental conditions

Temperature (K)	Sample path length of the cell (cm)	Maximum density of the gas (amagat)	Number of gas densities studied
77	194.9	50	12
196	195.1	60	15
298	209.6	60	14

3.1. Absorption Profiles

Representative absorption profiles of the D_2 fundamental band in the pure D_2 gas at 77, 196, and 298 K are shown in Fig. 5, 6, and 7, respectively, by plotting the quantity $\log_{10} [I_0(\nu)/I(\nu)]$ against wavenumber ν. Three absorption profiles corresponding to different densities of the gas are chosen at each temperature in order to illustrate the main features of the profiles. The positions of the single transitions $O_1(J)$, $Q_1(J)$ and $S_1(J)$, calculated from the constants of the free D_2 molecule, are marked on the wavenumber axis. The rotational states J = 0, 1, and 2 at 77 K, 0, 1, 2, and 3 at 196 K and 0, 1, 2, 3 and 4 at 298 K were considered. As stated in Chapter 1, in the collision-induced fundamental band of D_2, the isotropic part of the polarizability of D_2 in the quadrupole-induction mechanism contributes to the intensity of the single transitions $O_1(J)$, $Q_1(J)$ $(J\neq0)$ and $S_1(J)$ and of the double transitions $Q_1(J) + Q_0(J)$ and $Q_1(J) + S_0(J)$. The electron overlap-induction mechanism, on the other hand, contributes mainly to the $Q_1(J)$ [i.e., $Q_{1\ \text{overlap}}(J)$] transitions. In Figs. 5, 6, and 7, the extent of different single and double transitions are marked over the absorption peaks. In Figs. 6 and 7, a marked dip in the Q branch which occurs at the position of the $Q_1(1)$ line (2991.5 cm^{-1}) at 196 and 298 K. For the profiles at 77 K the dip is not noticeable, whereas it shows very clearly in those at 196

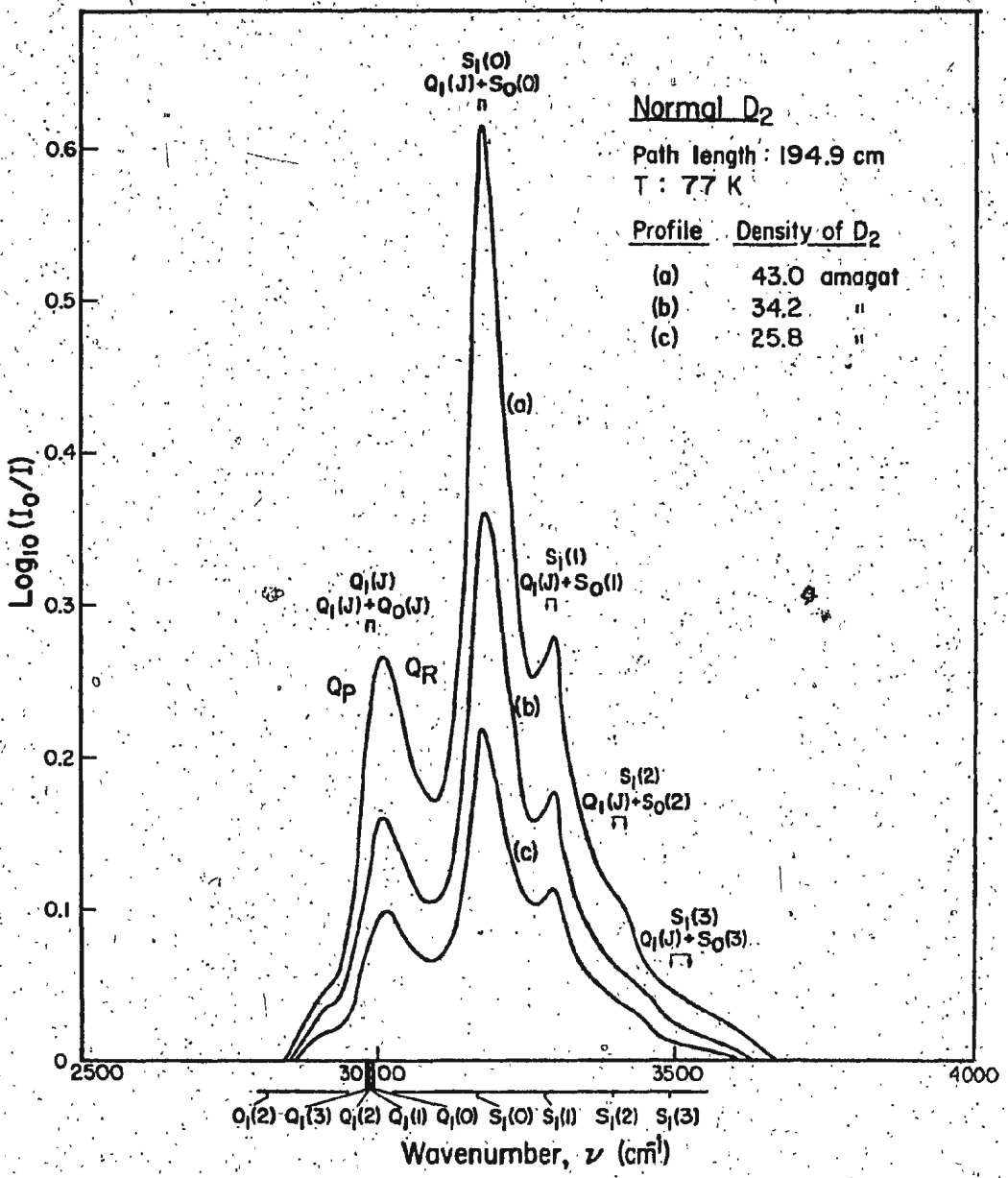

Fig. 5. Absorption profiles of the collision-induced fundamental band of normal D_2 at different densities of the gas at 77 K.

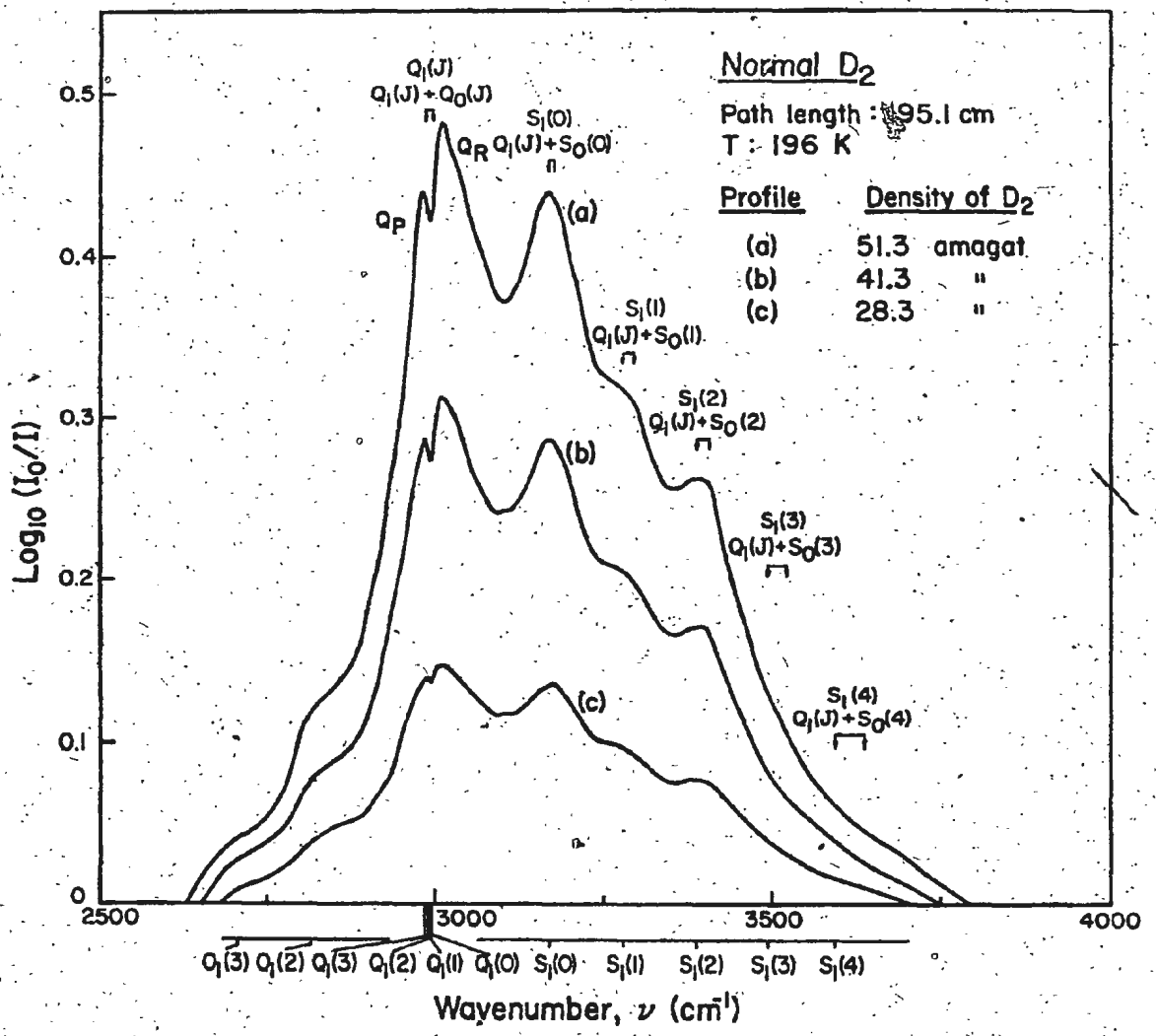

Fig. 6. Absorption profiles of the collision-induced fundamental band of normal D_2 at different densities of the gas at 196 K.

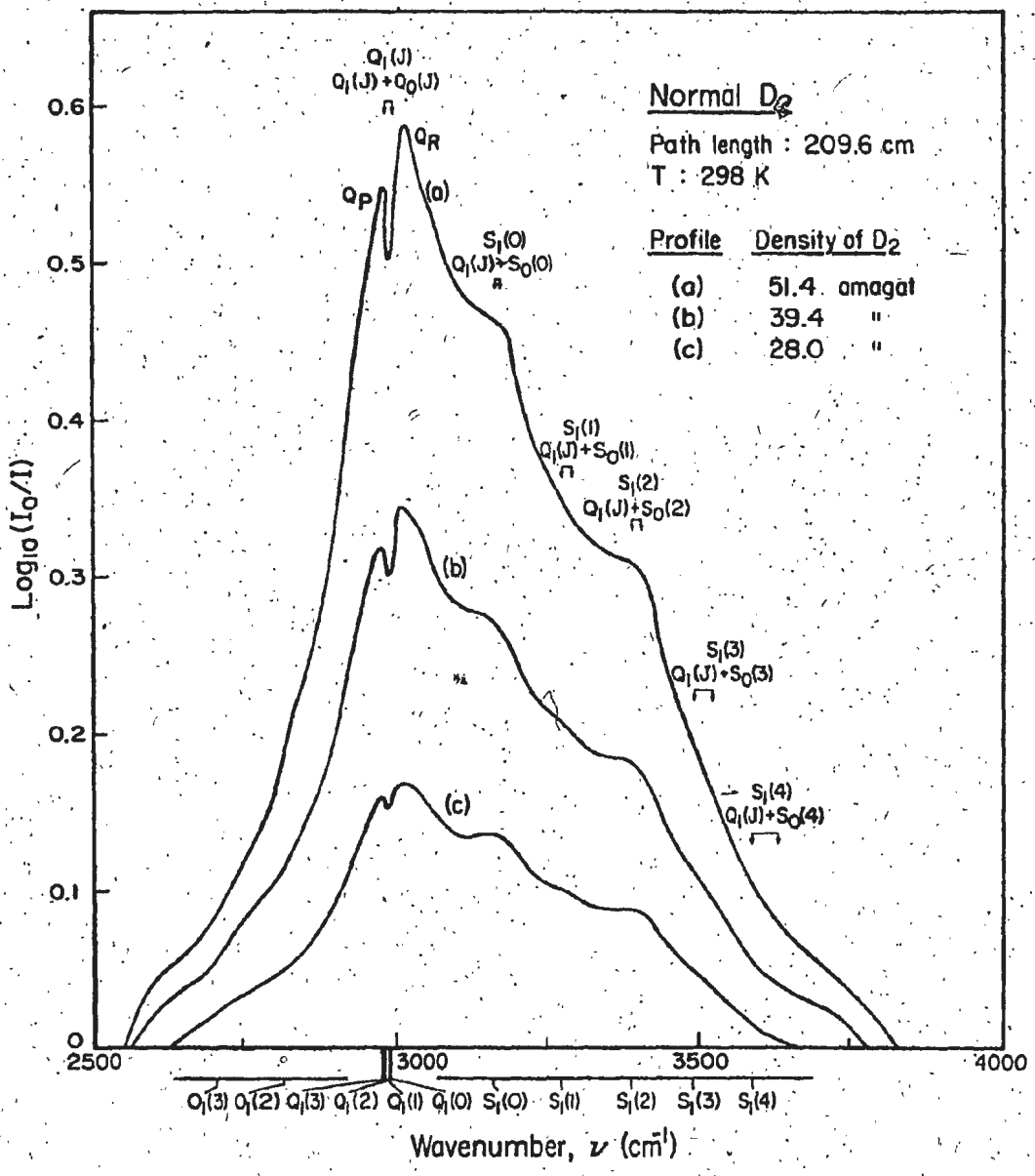

Fig. 7. Absorption profiles of the collision-induced fundamental band of normal D_2 at different densities of the gas at 298 K.

and 298 K at which the separation $\Delta\nu_{PR}^{max}$ between the peaks of the low and high wavenumber components Q_P and Q_R of the dip increases slightly with density. The dip in the Q branch was explained by Van Kranendonk (1968) in terms of the phenomenon of intercollisional interference occurring between overlap dipole moments in successive collisions. The widths of the individual components in collision-induced spectra have a characteristic dependence on the temperature. Although this dependency is different for the components arising from different induction mechanisms, the widths are in general relatively broad at higher temperature because the relative translational energy of the colliding pairs of molecules is large and hence the collision duration is small. At lower temperature the components are relatively narrow. The effect of low temperature on the spectra is clearly seen when one compares the absorption profiles at 77 K with those at higher temperatures.

3.2. Absorption Coefficients

The integrated absorption coefficient $\int\alpha(\nu)d\nu$ of the band (see section 2.5) can be expanded in a power series of the gas density ρ_a (= ρ_{D_2}) by the relation

$$\int\alpha(\nu)d\nu = \alpha_{1a}\,\rho_a^2 + \alpha_{2a}\,\rho_a^3 + \ldots, \qquad (2)$$

or

$$(1/\rho_a^2)\int\alpha(\nu)d\nu = \alpha_{1a} + \alpha_{2a}\,\rho_a + \ldots, \qquad (3)$$

where α_{1a} (cm^{-2} $amagat^{-2}$) and α_{2a} (cm^{-2} $amagat^{-3}$) are the binary and ternary absorption coefficients, respectively. Plots of $(1/\rho_{D_2}^2) \int \alpha(\nu) d\nu$ against ρ_{D_2} for the three experimental temperatures are shown in Fig. 8, where the intercepts and slopes were obtained from a linear least-squares fit of the data. The intercepts and slopes give the binary and ternary absorption coefficients, respectively, and the values of these are given in Table II. It is noted that the binary absorption coefficients are in general three orders of magnitude larger than the ternary absorption coefficients, indicating that the binary collisions contribute predominantly to the collision-induced absorption.

The absorption coefficient can also be expressed in the form

$$c \int \tilde{\alpha}(\nu) d\nu = \tilde{\alpha}_{1a} \rho_a^2 n_0^2 + \tilde{\alpha}_{2a} \rho_a^3 n_0^3 + \ldots , \qquad (4)$$

where c is the speed of light, $\tilde{\alpha}(\nu) = \alpha(\nu)/\nu$ and n_0, Loschmidt's number = 2.687×10^{19} cm^{-3}. The new binary and ternary absorption coefficients are related to the previous ones by the relations

$$\tilde{\alpha}_{1a} \ (cm^6 \ s^{-1}) = (c/n_0^2) \ \alpha_{1a} / \ \bar{\nu} , \qquad (5)$$

and

$$\tilde{\alpha}_{2a} \ (cm^9 \ s^{-1}) = (c/n_0^3 \ \alpha_{2a} / \ \bar{\nu} , \qquad (6)$$

where the band center $\bar{\nu}$ is given by

$$\bar{\nu} = \int \alpha(\nu) d\nu \ / \int \alpha(\nu) \nu^{-1} \ d\nu . \qquad (7)$$

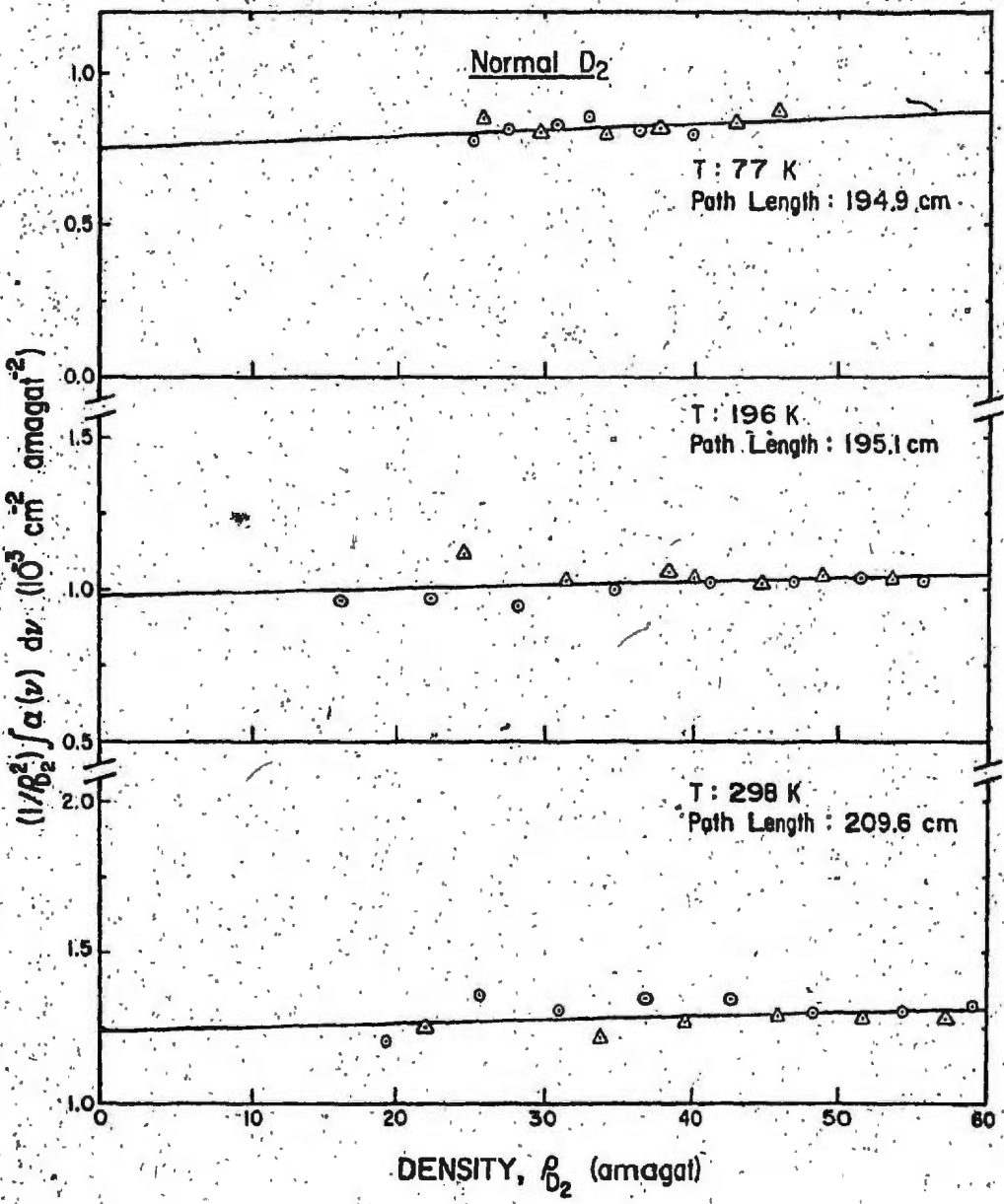

Fig. 8. Plots of $(1/\rho_{D_2}^2)\int\alpha(\nu)d\nu$ vs. ρ_{D_2} for the absorption profiles at 77, 196, and 298 K.

TABLE II. Absorption coefficients[a] of the fundamental band of normal D_2 at 77, 196, and 298 K

T (K)	Binary absorption coefficient α_{1a} (10^{-3} cm^{-2} amagat^{-2})	$\tilde{\alpha}_{1a}$ (10^{-35} cm^{6} sec^{-1})	Ternary absorption coefficient α_{2a} (10^{-6} cm^{-2} amagat^{-3})	Reference
77	0.75 ± 0.04	0.98 ± 0.05	1.9 ± 1.3	Present work
	0.57[b]	0.75		Watanabe and Welsh (1965)
196	0.97 ± 0.04	1.28 ± 0.05	1.3 ± 0.9	Present work
298	1.25 ± 0.04	1.66 ± 0.05	1.1 ± 1.0	Present work
	1.06 ± 0.02	1.40 ± 0.02	0.8 ± 0.2	Reddy and Cho (1965)

[a]Errors quoted are standard deviations.

[b]From published graph.

The average values of $\bar{\nu}$ are 3177, 3146, and 3122 cm^{-1} for the absorption profiles at 77, 196, and 298 K, respectively. The values of $\tilde{\alpha}_{1a}$ for the band are also included in Table II. Also included in this table are the values of the absorption coefficients obtained by previous researchers for comparison.

We note here that the binary absorption coefficients of the D_2 fundamental band at 77 and 298 K determined by earlier researchers are smaller by 23% and 15%, respectively, from the corresponding quantities obtained in the present work. The value of $\tilde{\alpha}_{1a}$ at 77 K by Watanabe and Welsh (1965) was inferred by us from their plot of $\tilde{\alpha}_{1a}$ versus temperature in the range 24 to 77 K, which shows a considerable scatter. In the present work the absorption coefficients of the band at 77 K were obtained from the profiles of the band at 12 different densities in the range 20 to 50 amagat. The room temperature value of $\tilde{\alpha}_{1a}$ of the band was obtained by Reddy and Cho (1965) by extrapolation, to zero density, of the data of the band studied at 6 gas densities in the range 85 to 200 amagat. However, in the present experiments the absorption coefficients of the band at room temperature were obtained from the experimental absorption profiles at 14 different densities in the range 20 to 60 amagat. It is obvious that our lower density data are expected to give more accurate extrapolation. Thus our present values of the absorption coefficients of the band are considered to be more accurate than those reported in earlier works.

CHAPTER 4

ANALYSIS OF THE ABSORPTION PROFILES

Collision-induced absorption of the fundamental band of a symmetric diatomic gas occurs mainly as a result of a short-range electron-overlap interaction and a long-range quadrupolar interaction. In the collision process, the induced dipole moment due to the overlap induction contributes principally to the Q branch transitions and the one due to the quadrupolar induction contributes to various single and double transitions in the O, Q, and S branches (see Chapter 1 for details). In the present chapter we describe a method of profile analysis which enables us to separate out the contributions of the overlap and quadrupolar transitions from the total absorption of the band and to obtain the characteristic half-widths of the spectral lines at the experimental temperatures.

4.1. Line Shape Functions

The absorption coefficient $\tilde{\alpha}(\nu)$ $(= \alpha(\nu)/\nu)$ at given wavenumber ν of the fundamental band is given by the relation (Van Kranendonk, 1968; see also Mactaggart and Welsh, 1973; Reddy et al., 1977; and Sen et al., 1980)

$$\tilde{\alpha}(\nu) = \sum_{m,n} \left\{ \frac{\tilde{a}^0_{nm}}{1 + \exp(-hc\Delta\nu/kT)} \right\} W_n(\Delta\nu), \qquad (8)$$

where n stands for the induction mechanism, subscripts o and q represent respectively the overlap and quadrupolar inductions, m represents a specific transition arising from a given mechanism, $\tilde{\alpha}^0_{nm}$ is a parameter indicating the maximum absorption coefficient (which is fictitious for the overlap components) at the molecular wavenumber ν_m, $W_n(\Delta\nu)$, with $\Delta\nu = \nu - \nu_m$, represents the line shape function of the n-type of mechanism; h, c, and k are the fundamental constants, and T is the absolute temperature. Spectral transitions arising from a given type of induction mechanism can be represented by the same line shape function (Poll, 1961). The factor $1 + \exp(-hc\Delta\nu/kT)$ on the right side of Eq. (8) converts the symmetrized line form $\tilde{\alpha}_{nm} W_n(\Delta\nu)$ into the observed asymmetric line shape. In this equation, the line shape function for the overlap transitions is represented by

$$W_o(\Delta\nu) = W^0_o(\Delta\nu)\, D(\Delta\nu), \qquad (9)$$

where

$$W^0_o(\Delta\nu) = (2\Delta\nu/\delta_d)^2 K_2(2\Delta\nu/\delta_d). \qquad (10)$$

Here $W^0_o(\Delta\nu)$ is the Levine-Birnbaun expression (Levine and Birnbaun, 1967), K_2 is the modified Bessel function of the second kind and δ_d is the intracollisional half-width at half-height. The function $D(\Delta\nu)$ is the Van Kranendonk's expression for the intercollisional part which is represented by (Van Kranendonk, 1968; see also Lewis, 1976 and

the references therein)

$$D(\Delta\nu) = 1 - \gamma[1 + (\Delta\nu/\delta_c)^2]^{-1} , \qquad (11)$$

where δ_c is the intercollisional half-width at half-height and γ is a constant which is usually taken as unity to give zero absorption at the dip occurring at the molecular wavenumber ν_m. The line shape functions $D(\Delta\nu)$, $W_o^0(\Delta\nu)$, $W_o(\Delta\nu)$ and $\tilde{\alpha}(\nu)$ of an overlap-induced transition are schematically represented in Fig. 9.

The line shape function of the quadrupolar transitions is represented by the dispersion-type (i.e., Lorentz-type) function

$$W_q(\Delta\nu) = 1/\{1 + (\Delta\nu/\delta_q)^2\} , \qquad (12)$$

where δ_q is the quadrupolar half-width at half-height.

4.2. Relative Intensities

The absorption coefficient of the m^{th} component of the overlap-induced transitions, i.e., $Q_{1\ \text{overlap}}(J)$, is proportional to the normalized Boltzmann factor P_J (Van Kranendonk, 1968), i.e.,

$$\tilde{\alpha}_{om}^0 \propto P_J , \qquad (13)$$

where

$$P_J = \frac{g_T(2J+1)\exp(-E_J/kT)}{\Sigma_J g_T(2J+1)\exp(-E_J/kT)} , \qquad (14)$$

and $\Sigma_J P_J = 1$. In Eq. (14), the nuclear statistical weight

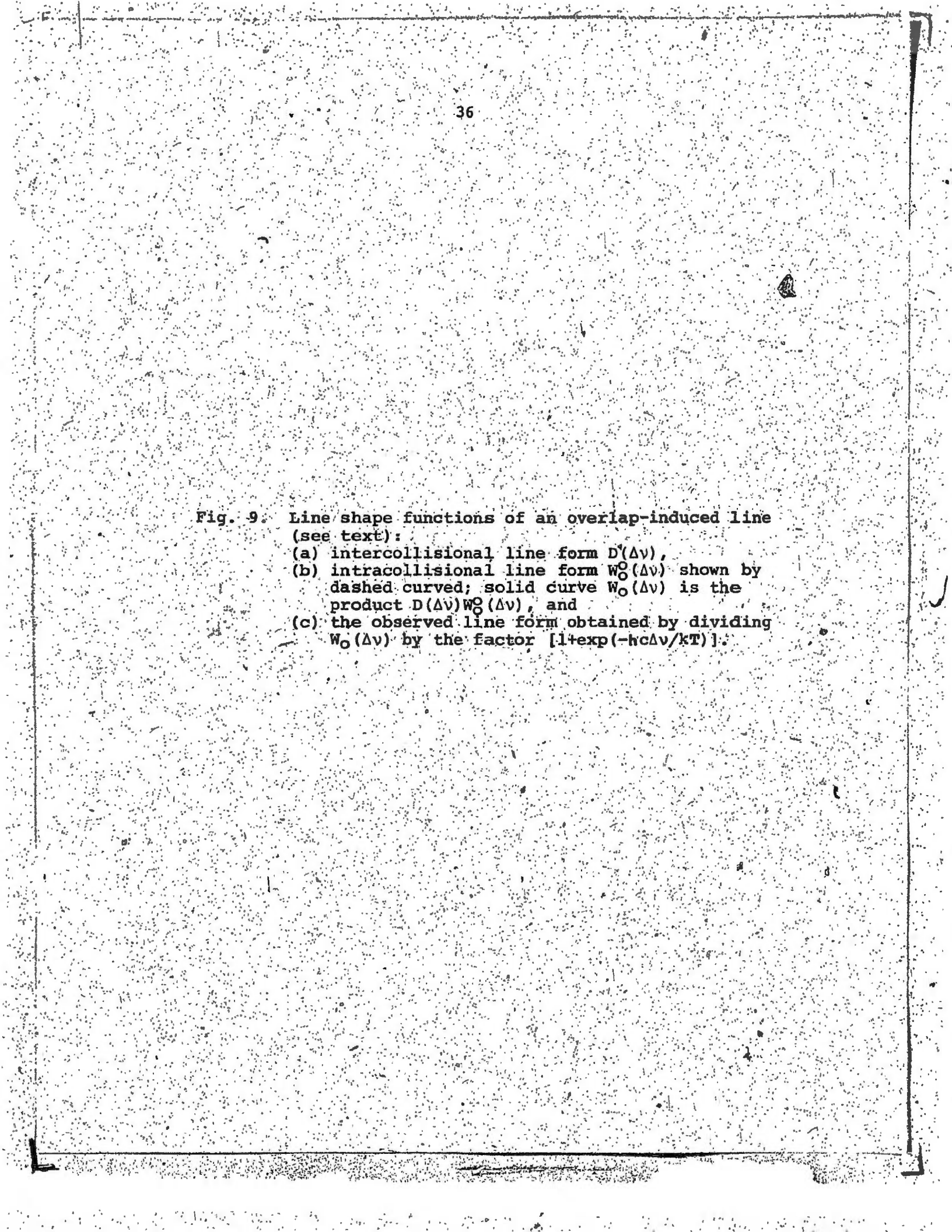

Fig. 9. Line shape functions of an overlap-induced line (see text):
(a) intercollisional line form $D(\Delta\nu)$,
(b) intracollisional line form $W_o^o(\Delta\nu)$ shown by dashed curved; solid curve $W_o(\Delta\nu)$ is the product $D(\Delta\nu)W_o^o(\Delta\nu)$, and
(c) the observed line form obtained by dividing $W_o(\Delta\nu)$ by the factor $[1+\exp(-hc\Delta\nu/kT)]$.

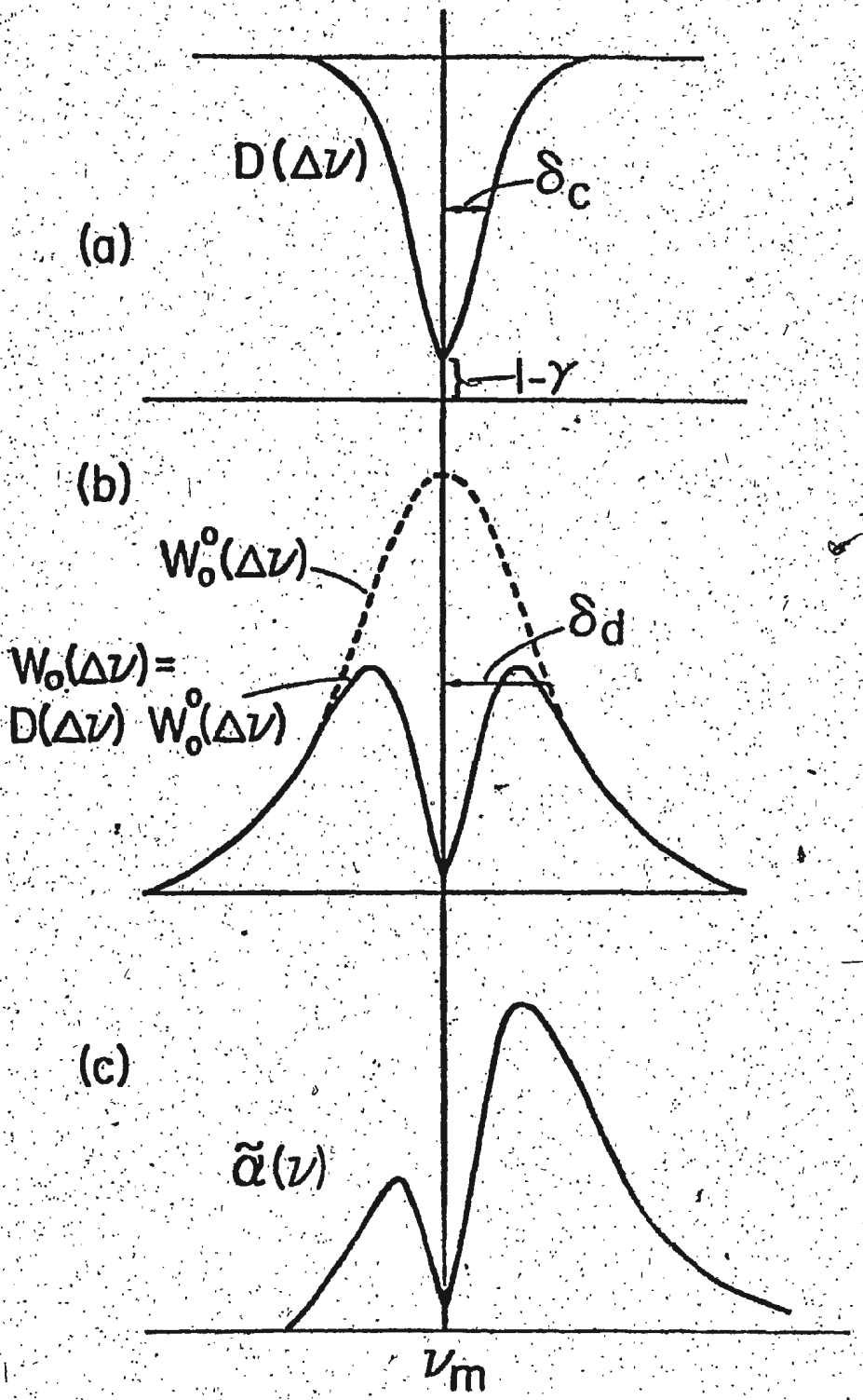
D(Δν)
δc
(a)
1-γ
(b)
W°o(Δν)
δd
Wo(Δν)=
D(Δν) W°o(Δν)
(c)
α̃(ν)
νm
Wavenumber

factor g_T is 6 and 3 for the even and odd J rotational states, respectively, of the D_2 molecule and E_J is the rotational energy of the J^{th} level calculated from the constants of the free D_2 molecule. Equation (14) is applicable to equilibrium D_2. For normal deuterium in which the conversion of para to ortho or vice versa is forbidden, the following relation is satisfied:

$$\Sigma_{\text{even } J} P_J / \Sigma_{\text{odd } J} P_J = 2/1. \qquad (15)$$

The relative intensities of the overlap transitions of the D_2 fundamental band at 77 K were expressed in terms of the intensity of Q_1 overlap(0) and those at 196 and 298 K were expressed in terms of that of Q_1 overlap (2). These values are presented in Table III.

The integrated binary absorption coefficient of the m^{th} quadrupolar transition of the $O_1(J)$, $Q_1(J)$ $(J\neq 0)$, $Q_1(J) + Q_0(J)$, $S_1(J)$ and $Q_1(J) + S_0(J)$ groups is given by (Poll, 1971)

$$\tilde{\alpha}_{qm} = K \sum_{J_1,J_2} P_{J_1} P_{J_2} [C(J_1 2 J_1'; 00)^2 \langle v_1' J_1' | Q_1 | 0 J_1 \rangle^2 C(J_2 0 J_2'; 00)^2$$

$$\times \langle v_2' J_2' | \alpha | 0 J_2 \rangle^2 + C(J_1 0 J_1'; 00)^2 \langle v_1' J_1' | \alpha_1 | 0 J_1 \rangle^2$$

$$\times C(J_2 2 J_2'; 00)^2 \langle v_2' J_2' | Q_2 | 0 J_2 \rangle^2], \qquad (16)$$

where K is given by

$$K = (4\pi^2 / 3hc)\, e^2\, a_o^5\, n_o^2\, (a_o/\sigma)^5\, J \qquad (17)$$

TABLE III

Relative intensities* of the overlap and quadrupolar transitions of the fundamental band of D_2

Transition	Wavenumber (cm^{-1})	Relative intensity		
		77 K	196 K	298 K
Overlap Transitions				
$Q_1(5)$	2962.18	-	-	0.0360
$Q_1(4)$	2972.61	0.0001	0.0858	0.2431
$Q_1(3)$	2980.99	0.0052	0.1892	0.2960
$Q_1(2)$	2987.29	0.1761	1.0000	1.0000
$Q_1(1)$	2991.50	0.5829	0.7204	0.5336
$Q_1(0)$	2993.61	1.0000	0.7446	0.4748
Quadrupolar Transitions				
$Q_1(4)$	2572.65	-	0.0525	0.2375
$Q_1(3)$	2693.97	0.0019	0.0958	0.2383
$Q_1(2)$	2814.55	0.0476	0.3640	0.5709
$Q_1(4)$	2972.61	-	0.0354	0.1571
$Q_1(4)+Q_0(J)$	2972.61	-	0.0178	0.0840
$Q_1(3)$	2980.99	0.0016	0.0797	0.1956
$Q_1(3)+Q_0(J)$	2980.99	0.0006	0.0392	0.1020

TABLE III (continued)

Transition	Wavenumber (cm^{-1})	Relative intensity		
		77 K	196 K	298 K
$Q_1(2)$	2987.29	0.0590	0.4502	0.7059
$Q_1(2)+Q_0(J)$	2987.29	0.0185	0.2065	0.3434
$Q_1(1)$	2991.51	0.2731	0.4533	0.5266
$Q_1(1)+Q_0(J)$	2991.51	0.0611	0.1483	0.1827
$Q_1(0)$	2993.61	0	0	0
$Q_1(0)+Q_0(J)$	2993.61	0.1045	0.1527	0.1620
$Q_1(5)+S_0(0)$	3141.25	-	0.0015	0.0091
$Q_1(4)+S_0(0)$	3151.68	-	0.0242	0.0610
$Q_1(3)+S_0(0)$	3160.06	0.0019	0.0449	0.0741
$Q_1(2)+S_0(0)$	3166.36	0.0650	0.2365	0.2494
$S_1(0)$	3166.36	1.0000	1.0000	1.0000
$Q_1(1)+S_0(0)$	3170.57	0.2142	0.1698	0.1327
$Q_1(0)+S_0(0)$	3172.68	0.3668	0.1749	0.1177
$Q_1(5)+S_0(1)$	3259.71	-	0.0008	0.0062
$Q_1(4)+S_0(1)$	3270.15	-	0.0119	0.0413
$Q_1(3)+S_0(1)$	3278.52	0.0007	0.0262	0.0502
$S_1(1)$	3278.52	0.3130	0.5197	0.6037
$Q_1(2)+S_0(1)$	3284.83	0.0228	0.1379	0.1690
$Q_1(1)+S_0(1)$	3289.04	0.0754	0.0990	0.0899
$Q_1(0)+S_0(1)$	3291.15	0.1289	0.1020	0.0797

TABLE III (continued)

Transition	Wavenumber (cm^{-1})	Relative intensity 77 K	196 K	298 K
$Q_1(5)+S_0(2)$	3376.83	-	0.0010	0.0099
$Q_1(4)+S_0(2)$	3387.26	-	0.0143	0.0669
$S_1(2)$	3387.26	0.0722	0.5504	0.8632
$Q_1(3)+S_0(2)$	3395.64	0.0002	0.0313	0.0811
$Q_1(2)+S_0(2)$	3401.94	0.0059	0.1652	0.2733
$Q_1(1)+S_0(2)$	3406.15	0.0196	0.1186	0.1454
$Q_1(0)+S_0(2)$	3408.26	0.0336	0.1222	0.1289
$S_1(3)$	3492.09	0.0018	0.0854	0.2095
$Q_1(5)+S_0(3)$	3492.09	-	0.0002	0.0027
$Q_1(4)+S_0(3)$	3502.52	-	0.0025	0.0185
$Q_1(3)+S_0(3)$	3510.90	-	0.0055	0.0224
$Q_1(2)+S_0(3)$	3517.20	0.0002	0.0292	0.0756
$Q_1(1)+S_0(3)$	3521.41	0.0005	0.0209	0.0402
$Q_1(0)+S_0(3)$	3523.52	0.0009	0.0216	0.0357

*The relative intensities given are valid within each of the overlap and quadrupolar groupings.

In Eq. (16), subscripts 1 and 2 refer to the molecules one and two of the colliding pair, the quantities $C(J\lambda J';00)$ with $\lambda = 0$ and 2 are the Clebsch-Gordan coefficients, $\langle 0J|\alpha|v'J'\rangle$ are the matrix elements of the polarizability and $\langle 0J|Q|v'J'\rangle$ are the matrix elements of the quadrupole moment. For the fundamental band, $v_1' = 1$ and $v_2' = 0$ or vice versa. In Eq. (17), a_o is the first Bohr radius, e is the electron charge, n_o is the Loschmidt's number, and σ is the Lennard-Jones intermolecular diameter. The quantity J is a temperature-dependent dimensionless integral and represents the average dependence of the square of the quadrupole-induced dipole moment on the intermolecular separation and has been discussed in detail elsewhere (Van Kranendonk, 1958; see also Sen et al., 1980). For the calculation of the relative intensities of the quadrupolar intensities, estimation of the numerical value of K is not necessary. The values of the matrix elements of the polarizability of D_2 were obtained by a scaling procedure from those of H_2 given by Poll (1971; private communication) and the values of the matrix elements of the quadrupole moment of D_2 were taken from Birnbaun and Poll (1969). Finally, the relative intensities of the quadrupolar components of the band expressed in terms of the intensity of the $S_1(0)$ component at all the three experimental temperatures, are presented in Table III.

4.3. Computational Procedure and Results of Profile Analysis

The aim of the profile analysis is to obtain satisfactory fits between the experimental absorption profiles and the synthetic profiles, computed from the functional relation for $\tilde{\alpha}(\nu)$ $[= (2.303 / \ell\nu) \log_{10}\{I_o(\nu) / I(\nu)\}]$ as given by Eq. (8) with the appropriate line shape functions for the overlap and quadrupolar groups of transitions, and thereby to separate the overlap and quadrupolar contributions to the band intensity and to derive certain characteristic molecular parameters of the collision process. The maximum intensity factors $\tilde{\alpha}^0_{om}$ and $\tilde{\alpha}^0_{qm}$, the half-width parameters δ_d, δ_c, and δ_q were the adjustable parameters in the program written for the IBM 370/158 computer. To account for any possible perturbations in the energy levels of the D_2 molecule, a shift parameter for the molecular wavenumber ν_m was also introduced in the computer program.

Several trial values of the adjustable parameters were used for the computation of the synthetic profile until the best nonlinear least-squares fits to the experimental profiles were obtained. For the best fits of computed profiles to the experimental profiles the computer also listed separately the overlap and quadrupolar contributions to the intensity of the band. An example of the profile analysis of the fundamental band for a density of 37.8 amagat at 77 K is shown in Fig. 10. In this figure all the individual overlap and quadrupolar components, except

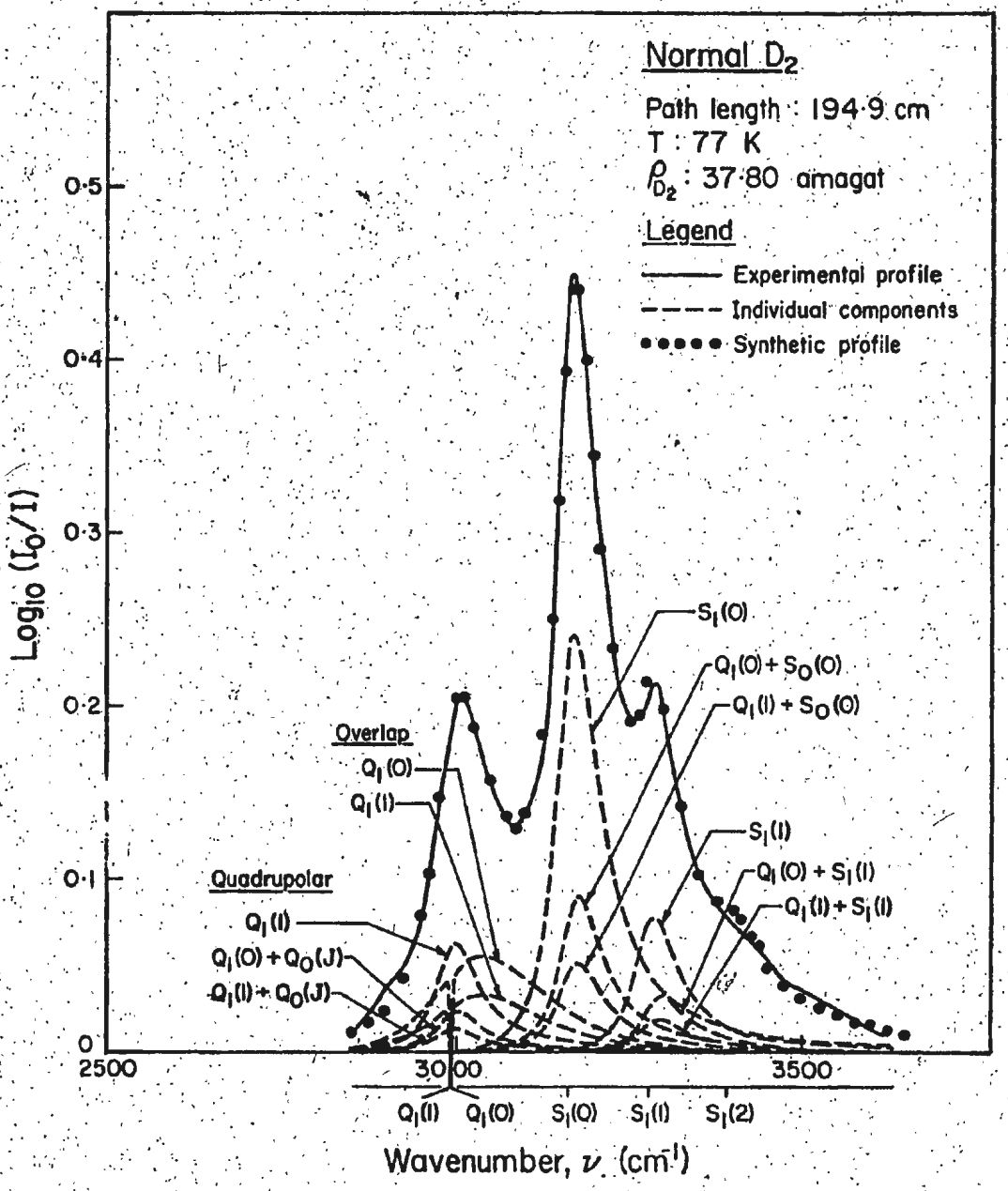

Fig. 10. Analysis of an absorption profile of the D_2 fundamental band at 77 K. The solid curve is the experimental profile. The dashed curves represent the computed individual overlap- and quadrupolar-induced components and the dots represent the summation of these. For the sake of clarity, the weaker components with J=2 are not shown. Note that the quadrupolar-induced components $Q_1^*(0)$ and $Q_1(J)+Q_0(0)$ are forbidden.

the weaker ones with J = 2, are shown; the synthetic absorption profile agrees closely with the experimental profile in the entire region of the band. Examples of profile analysis of the fundamental band of D_2 at 196 and 298 K are shown in Figs. 11 and 12. In these figures, the individual components are not shown but the total overlap and quadrupolar contributions are plotted separately. It is seen from these figures that there is good agreement between the experimental and synthetic absorption profiles. For all the absorption profiles analyzed in this work best fits were obtained without any shift in ν_m. The results obtained from the profile analysis are listed in Table IV. From the values of the characteristic half-widths δ_d and δ_q, the collision durations τ_d and τ_q were calculated from the relations $\tau_d = 1/2\pi c\delta_d$ and $\tau_q = 1/2\pi c\delta_q$ and are also listed in this table. It is noted that the overlap contributions to the intensity of the band increases from 21% at 77 K to 46% at 298 K and the quadrupolar contribution decreases from 79% to 54%.

The intercollisional half-width δ_c is expected to increase with density as well as temperature of the gas. As the present experiments were limited only up to 60 amagat of the D_2 gas, the data obtained from the profile analysis are not sufficient to ascertain a definite density dependence at a given temperature. The average values of δ_c at 77, 196, and 298 K are 0.9, 1.1, and 1.5 cm^{-1},

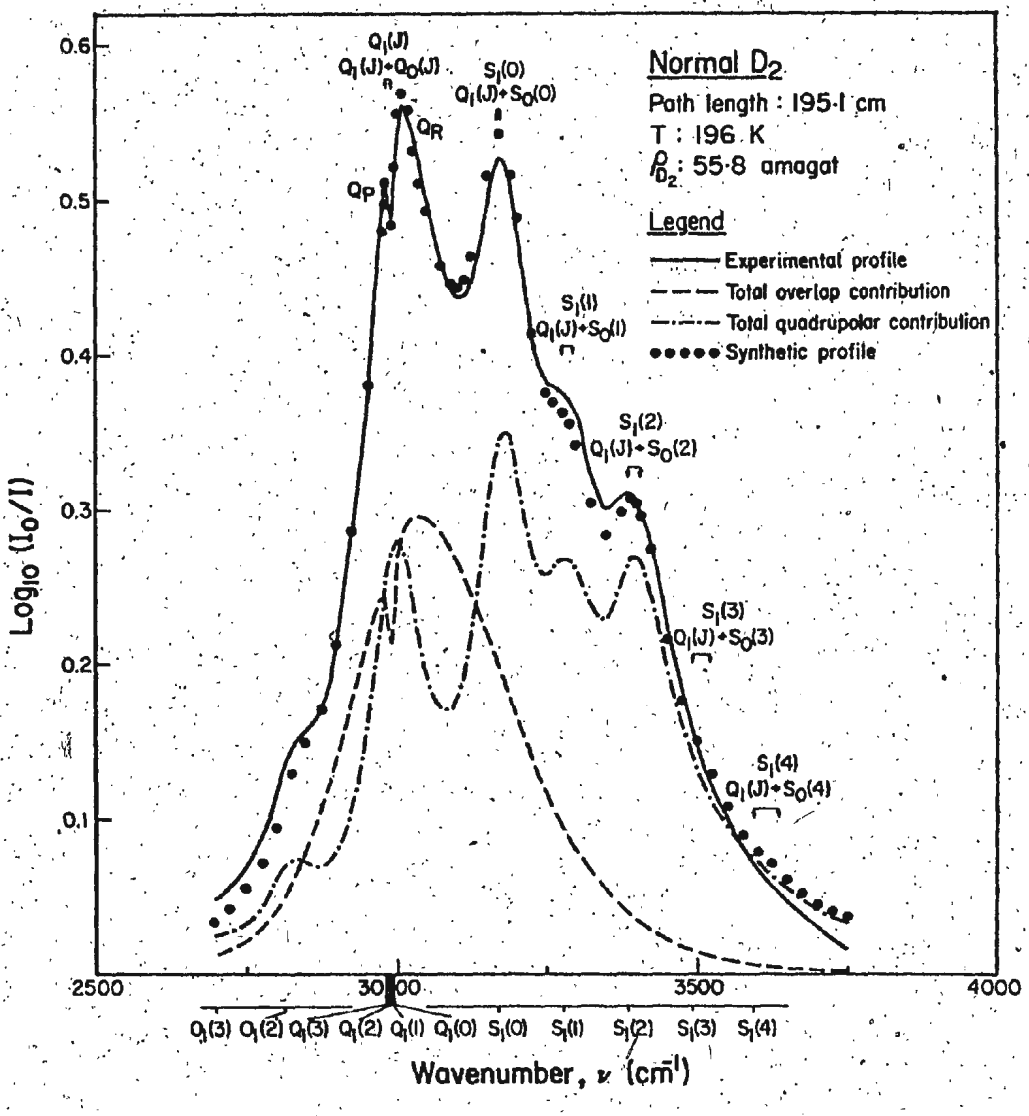

Fig. 11. Analysis of an absorption profile of the D_2 fundamental band at 196 K. Here J takes the values 0 - 4. The solid curve is the experimental profile. The computed contributions of the overlap and quadrupolar interactions to the total absorption intensity of the band are shown by the dashed and dot-dashed curves, respectively; the summation of these is represented by the dots.

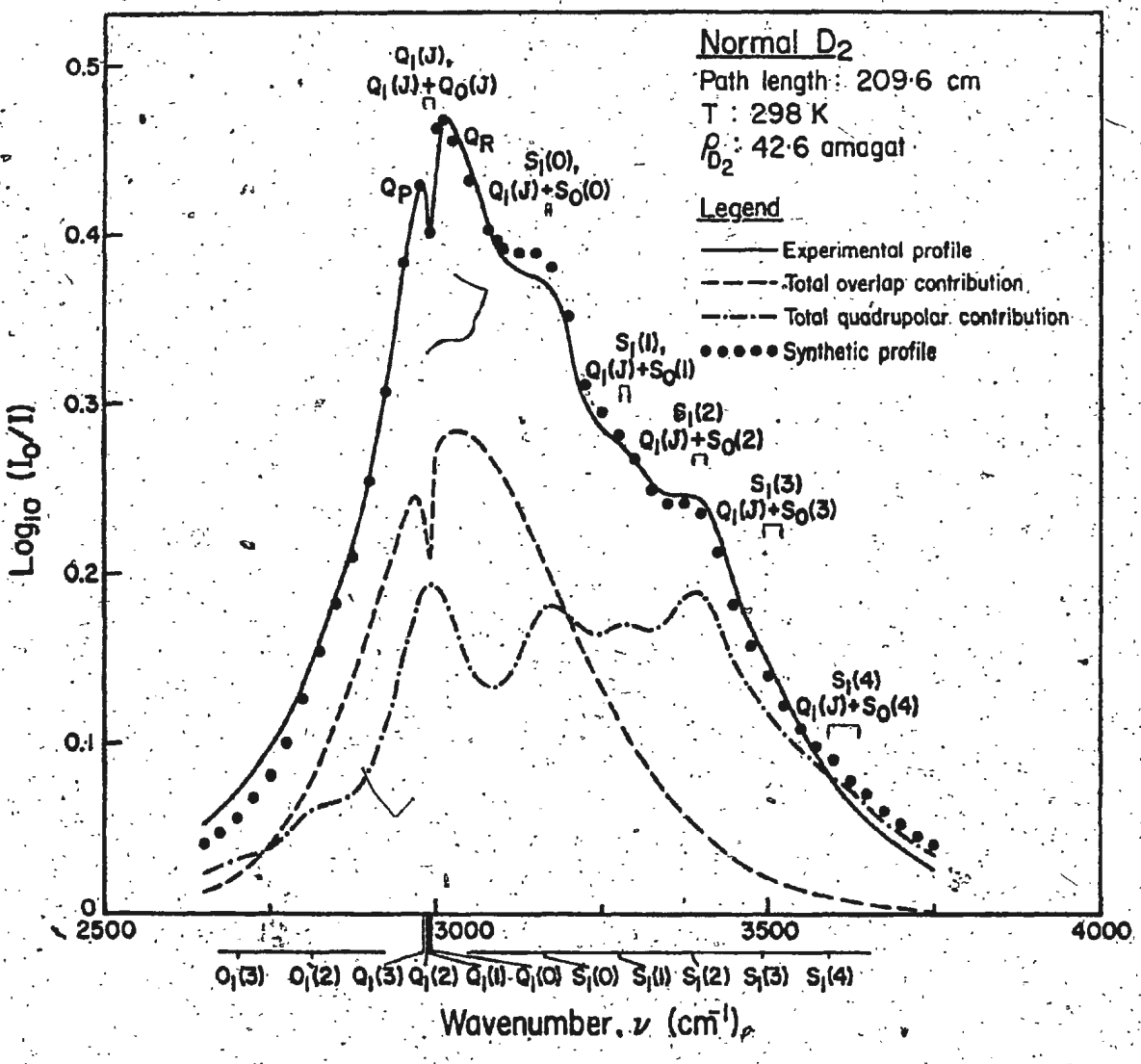

Fig. 12. Analysis of an absorption profile of the D_2 fundamental band at 298 K. For other details see caption of Fig. 11.

TABLE IV. Results of profile[a] analysis of normal D_2 gas.

T (K)	Intracollisional half-width δ_d (cm^{-1})	Collision duration τ_d (10^{-14} sec)	Quadrupolar half-width δ_q (cm^{-1})	Collision duration τ_q (10^{-14} sec)	Overlap Contribution (%)	Quadrupolar Contribution (%)
77	102 ± 8	5.2	38 ± 1	14.0	21	79
196	158 ± 4	3.4	58 ± 2	9.2	38	62
298	179 ± 4	3.0	75 ± 7	7.1	46	54

[a]Errors shown are standard deviations.

respectively. The half-widths δ_d and δ_q are independent of density within the range of densities used but they show a characteristic dependence on temperature. Plots of δ_d and δ_q against $T^{\frac{1}{2}}$ presented in Fig. 13 show that δ_d and δ_q increase linearly with $T^{\frac{1}{2}}$ in a manner similar to those obtained for H_2-H_2 (Reddy et al., 1977) and HD-HD (Reddy and Prasad, 1977). The intercept of the upper line in Fig. 13 gives a value of 23 cm^{-1} which corresponds to the value of δ_d at T = 0. This value for D_2-D_2 is lower than the corresponding values of 133 cm^{-1} and 88 cm^{-1} for H_2-H_2 and HD-HD, respectively. A large value of δ_d at T = 0 means that the duration of the collision is still small at absolute zero temperature because the overlap induction occurs mainly in the region of the strong repulsive forces between the molecules of the colliding pairs. As a matter of fact, at T = 0 where all substances exist in the solid phase, the translational energy spectrum manifests itself in the form of a broad phonon energy spectrum of the crystal lattice. The straight line obtained from the plot of δ_q against $T^{\frac{1}{2}}$ for D_2-D_2 gives the relation $\delta_q = 4.35\sqrt{T}$. The corresponding relations for H_2-H_2 and HD-HD are $\delta_q = 6.16\sqrt{T}$ and $\delta_q = 4.65\sqrt{T}$, respectively. In all three cases the half-widths are thus proportional to the average relative velocities of the colliding pairs of molecules.

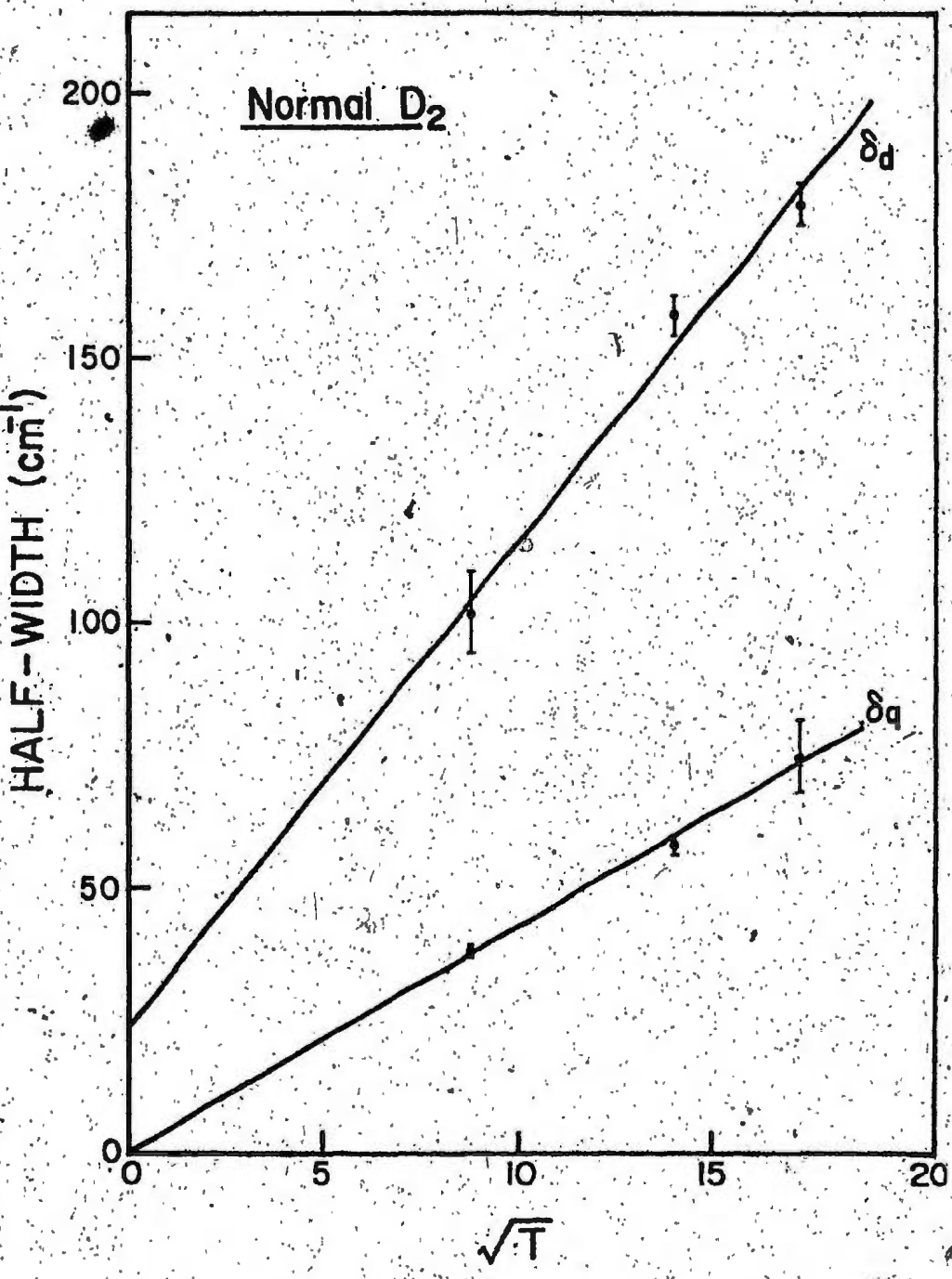

Fig. 13. Half-width parameters δ_d and δ_q against the square root of the absolute temperature T.

CHAPTER 5

OVERLAP PARAMETERS FOR THE D_2-D_2 COLLISION PAIRS

5.1. The Overlap Absorption Coefficients

Profile analysis described in Chapter 4 gave the integrated overlap absorption coefficients $\int\alpha_{overlap}(\nu)d\nu$ which can be represented by the relation that is analogous to Eq. (2)

$$\int\alpha_{overlap}(\nu)d\nu = \alpha_{1a\ overlap}\rho_a^2 + \alpha_{2a\ overlap}\rho_a^3 + \ldots \quad (18)$$

The quantities $(1/\rho_{D_2}^2)\int\alpha_{overlap}(\nu)d\nu$ when plotted against ρ_{D_2} in Fig. 14 are found to give linear dependence. The intercepts and slopes of the straight lines in this figure, obtained from linear least-squares fits of the data, gave values of the overlap binary and ternary absorption coefficients $\alpha_{1a\ overlap}$ (cm^{-2} $amagat^{-2}$) and $\alpha_{2a\ overlap}$ (cm^{-2} $amagat^{-3}$), respectively. Values of these coefficients and binary absorption coefficients $\tilde{\alpha}_{1a\ overlap}$ [$= (c/n_o^2) \times \alpha_{1a\ overlap}/\bar{\nu}$] expressed in units of $cm^6\ s^{-1}$ are given in Table V. The average values of the overlap band center $\bar{\nu}$ at 77, 196 and 298 K are 3061, 3074, and 3065 cm^{-1}, respectively.

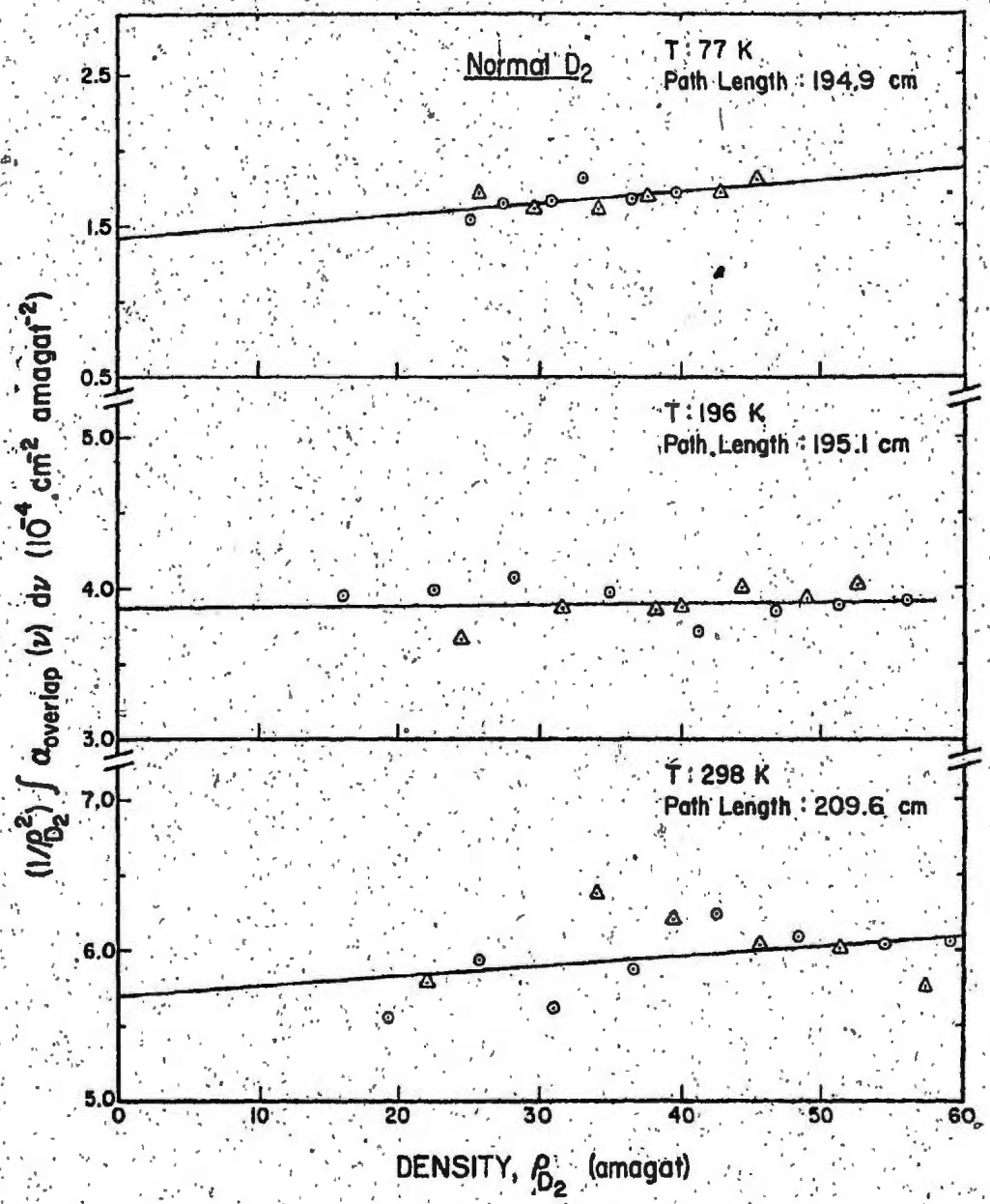

Fig. 14. Plots of $(1/\rho_{D_2}^2) \int \alpha_{overlap}(\nu)\, d\nu$ obtained from the profile analysis vs. ρ_{D_2} at 77, 196, and 298 K.

TABLE V. Absorption coefficients[a] of the overlap part of the fundamental band of normal D_2 at 77, 196, and 298 K.

T (K)	Binary absorption coefficient		Ternary absorption coefficient
	α_{1a} overlap (10^{-3} cm^{-2} amagat^{-2})	$\tilde{\alpha}_{1a}$ overlap (10^{-35} cm^{6} sec^{-1})	α_{2a} overlap (10^{-6} cm^{-2} amagat^{-3})
77	0.14 ± 0.01	0.19 ± 0.01	0.7 ± 0.3
196	0.39 ± 0.01	0.53 ± 0.01	0.1 ± 0.3
298	0.57 ± 0.02	0.77 ± 0.02	0.7 ± 0.5

[a]Errors shown are standard deviations.

5.2. Overlap Parameters for the D_2-D_2 Collision Pairs

The overlap binary absorption coefficient $\tilde{\alpha}_{1a\ \text{overlap}}$ of the fundamental band can be expressed as (Van Kranendonk, 1958)

$$\tilde{\alpha}_{1a\ \text{overlap}} = (8\pi^3 / 3h)\ \kappa_1^2 \int |\vec{M}_o(\vec{R})|^2\ g_o(\vec{R})\, d\vec{R}, \qquad (19)$$

where $\vec{M}_o = \langle (\partial \vec{\mu} / \partial r)_{r=r_o} \rangle$ is the variation of the induced overlap dipole moment $\vec{\mu}_{\text{overlap}}$ with respect to r at internuclear separation r_o, the quantity $\kappa_1 = \langle v=0 | r-r_o | v'=1 \rangle$ is the matrix element and $g_o(\vec{R})$ is the low density limit of the pair distribution function. The quantity $M_o(R)$ is assumed to decrease exponentially with intermolecular separation R and is represented as

$$M_o(R) = \xi \exp(-R/\rho) = \lambda e \exp[-(R-\sigma)/\rho], \qquad (20)$$

where the dimensionless quantity λ is given by

$$\lambda = (\xi/e)\ \exp(-\sigma/\rho). \qquad (21)$$

The quantity λe represents the amplitude of the overlap induced dipole moment when the intermolecular separation is σ corresponding to the Lennard-Jones intermolecular potential $V(\sigma) = 0$. As a matter of fact

$$\mu_{\text{overlap}}(\sigma) = \lambda e \sigma. \qquad (22)$$

The quantities ξ and ρ represent respectively the magnitude and the range of the scalar part of the overlap dipole

moment. On substitution of Eq. (20) in Eq. (19), we obtain

$$\tilde{\alpha}_{\text{la overlap}} = (8\pi^3/3h)\,|\langle 0|r-r_o|1\rangle|^2 \int \xi^2 \exp(-2R/\rho) g_o(R)\, 4\pi R^2 dR$$

$$= \{(\xi/e)\ \exp(-\sigma/\rho)\}^2$$

$$\times\ 4\pi \int_0^\infty \exp\{-2(R-\sigma)/\rho\}\, g_o(R)\, R^2\, dR$$

$$\times\ (8\pi^3/3h) e^2 |\langle 0|r-r_o|1\rangle|^2$$

$$= \lambda^2 \times 4\pi \int_0^\infty \exp\{-2(x-1)(\sigma/\rho)\}\, g_o(x) x^2\, dx$$

$$\times\ (8\pi^3/3h)\ e^2 \sigma^3 |\langle 0|r-r_o|1\rangle|^2$$

$$= \lambda^2\, I\, \tilde{\gamma}, \tag{23}$$

where $x = R/\sigma$ and $\tilde{\gamma}$ is given by

$$\tilde{\gamma} = (8\pi^3/3h) e^2 \sigma^3 |\langle 0|r-r_o||1\rangle|^2 \tag{24}$$

and has the dimensions of the binary absorption coefficient (i.e., $cm^6\ sec^{-1}$). The temperature dependent integral $I(T^*)$ is given by

$$I(T^*) = 4\pi \int_0^\infty \exp\{-2(x-1)(\sigma/\rho)\}\, g_o(x) x^2\, dx \tag{25}$$

It represents the average R- dependence of $M_o(R)$. The classical value of I, i.e., $I_{\text{classical}}$ can be obtained by calculating the integral given by Eq. (25), using the

classical pair distribution function

$$g_o(x) = \exp[-V^*(x)/T^*], \tag{26}$$

where $V^*(x) = V(x)/\varepsilon$, $V(x)$ being the Lennard-Jones intermolecular potential, which is represented as

$$V(x) = 4\varepsilon[x^{-12} - x^{-6}]. \tag{27}$$

Note that $T^* = kT/\varepsilon$ is the reduced temperature. The quantity ε is the depth of the potential well. Classical values are applicable at high temperatures. At intermediate temperatures where quantum effects should be included I can be expressed as

$$I = I_{cl} - \Lambda^{*2} I^{(2)} + \Lambda^{*4} I^{(4)} + \ldots, \tag{28}$$

where Λ^* $[= (h^2/2\, m_{00}\, \varepsilon\, \sigma^2)^{\frac{1}{2}}]$ is the reduced de Broglie wavelength, m_{00} being the reduced mass of the colliding pair of molecules. The integral I_{cl} depends on σ/ρ. To obtain the most probable value of σ/ρ for the D_2-D_2 collision pairs the following procedure (see Reddy and Chang, 1973) was used. The values of I_{cl} were calculated by a computer program for a series of values of σ/ρ in the range 0.070 to 0.140 at intervals of 0.002 for reduced temperatures T^* from 0.5 to 20.00 at intervals of 0.5. Quantum corrections $I^{(2)}$ and $I^{(4)}$ listed recently by Gibbs et al. (1979) were used to obtain I (Eq. 28). The quantity λ^2 was assumed to be independent of temperature. $\tilde{\gamma}$ was calculated from Eq. (24)

from the values of the matrix elements $\langle 0|r-r_o|1\rangle$ given by Poll (private communication). It is 3.937×10^{-32} cm^6 sec^{-1} for D_2-D_2. For a series of values of σ/ρ, I_{cl} and hence I were calculated and the corresponding calculated values of $\lambda^2 I$ as a function of T were fitted to the experimental values of $\lambda^2 I$. The criterion used for the best fit was that $\sum_i \delta_i^2$ where δ_i are the deviations of the calculated values of $\lambda^2 I$ from the corresponding experimental values, be a minimum. The results of such a fit are shown in Fig. 15. The values of σ/ρ and λ for D_2-D_2 obtained from the best fit are given in Table VI. Also included in this table are values of ρ, σ and $\mu_{overlap}(\sigma)$ [Eq. (22)]. The corresponding values of the collision pairs H_2-H_2 and HD-HD obtained by Reddy et al. (1977a, 1977b) are also included in Table VI.

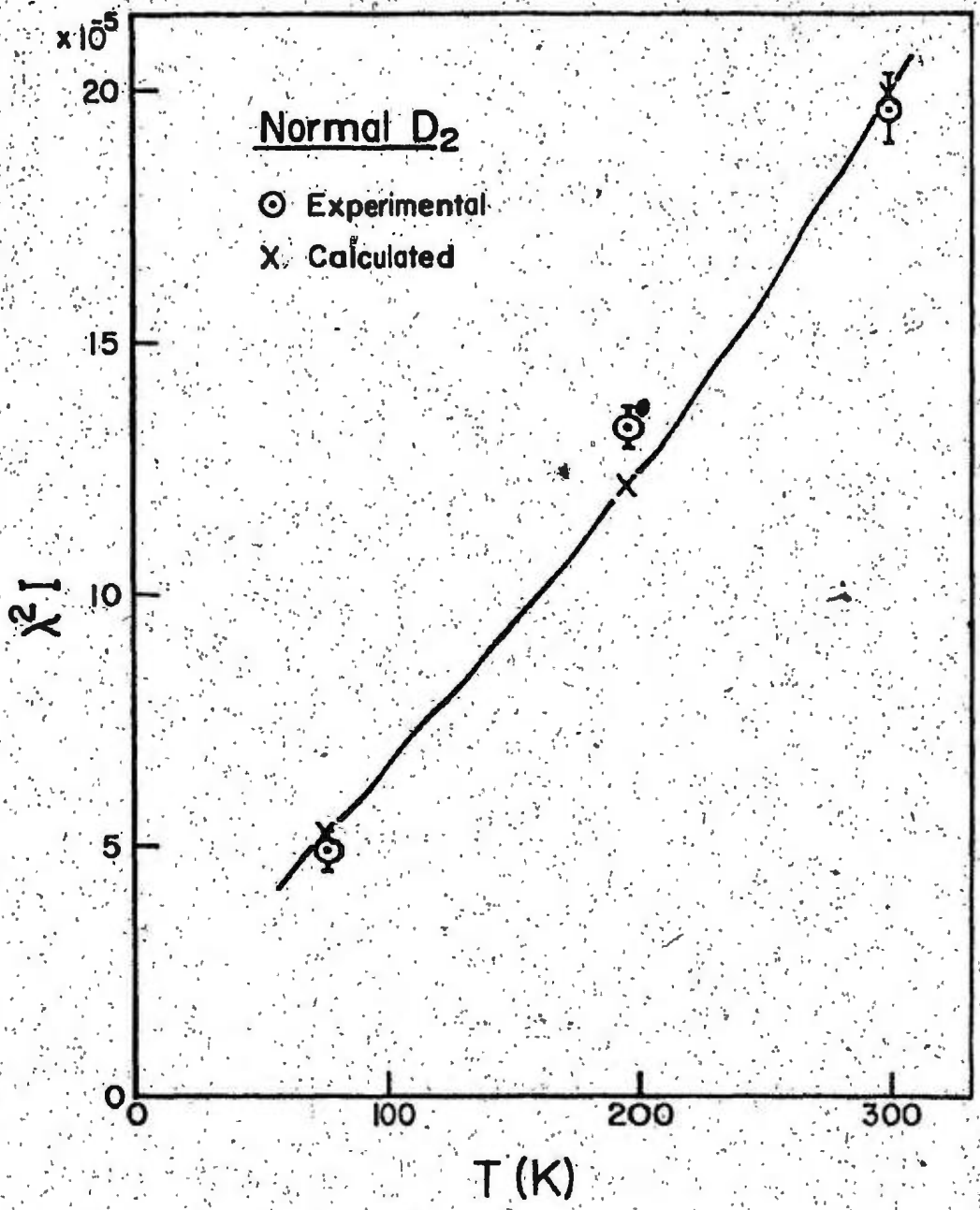

Fig. 15. Variation of $\lambda^2 I$ with absolute temperature T.

TABLE VI. Overlap parameters[a] for the H_2-H_2, HD-HD, and D_2-D_2 pairs.

Collision pair	ρ/σ	λ (10^{-3})	σ (Å)	ρ (Å)	$\mu_{overlap}(\sigma)$ (10^{-2} ea_0)	Reference
H_2-H_2	0.071	3.7	2.928	0.21	2.0	Reddy, Varghese, and Prasad (1977a)
HD-HD	0.074	4.7	2.928	0.22	2.6	Reddy and Prasad (1977b)
D_2-D_2	0.073	4.4	2.928	0.21	2.4	Present work

[a]The overlap parameters for the H_2-H_2 and HD-HD listed here differ slightly from the values given by Reddy et al. (1977a) and Reddy and Prasad (1977b). These parameters are now recalculated by using the values of the quantum corrections $I^{(2)}$ and $I^{(4)}$ recently reported by Gibbs et al. (1979).

REFERENCES

Birnbaum, A. and Poll, J.D. 1969. J. Atmos. Sci. 26, 943.

Chang, K.S. 1974. Ph.D. thesis, Memorial University of Newfoundland (unpublished).

Crawford, M.F., Welsh, H.L., and Locke, J.L. 1949. Phys. Rev. 75, 1607.

Gibbs, P.W., Hunt, J.L., and Poll, J.D. 1979. Can. J. Phys. 57, 981.

IUPAC Tables of Wavenumbers of Calibration of Infrared Spectrometers, 1977. (Ed. A.R.H. Cole, Pergamon, Oxford-New York, 2nd edition).

Kiss, Z.J., and Welsh, H.L. 1959. Can. J. Phys. 37, 1249.

Levine, H.B., and Birnbaum, G. 1967. Phys. Rev. 154, 72.

Lewis, J.C. 1976. Physica 82A, 500.

Mactaggart, J.W., and Welsh, H.L. 1973. Can. J. Phys. 51, 158.

McKellar, A.R.W., and Oka, T. 1978. Can. J. Phys. 56, 1315.

Michels, A., De Graff, W., Wassenaar, T., Levelt, J.M.H., and Louwerse, P. 1959. Physica 25, 25.

Michels, A., and Goudeket, M. 1941. Physica 8, 347.

Pai, S.T., Reddy, S.P., and Cho, C.W. 1966. Can. J. Phys. 44, 2893.

Poll, J.D. 1961. Ph.D. thesis, University of Toronto (unpublished).

Poll, J.D. 1971. In Proceedings I.A.U. Symposium 40 on Planetary Atmosphers, Marfa, Taxes, p. 384 (Reidel, Dordrecht, Holland).

Poll, J.D. Private communication.

Poll, J.D., and Wolniewicz, L. 1978. J. Chem. Phys. 68, 3053.

Prasad, R.D.G. 1976. Ph.D. thesis, Memorial University of Newfoundland (unpublished).

Rao, K.N., Humphreys, C.J., and Rank, D.H. 1966. Wavelength Standards in the Infrared (Academic Press, New York).

Reddy, S.P., and Cho, C.W. 1965. Can. J. Phys. 43, 793.

Reddy, S.P., and Chang, K.S. 1973. J. Mol. Spectrosc. 47, 22.

Reddy, S.P., and Kuo, C.Z. 1971. J. Mol. Spectrosc. 37, 327.

Reddy, S.P., and Prasad, R.D.G. 1977b. J. Chem. Phys. 66, 5259.

Reddy, S.P., Sen, A., and Prasad, R.D.G. 1980. J. Chem. Phys. June issue.

Reddy, S.P., Varghese, G., and Prasad, R.D.G. 1977a. Phys. Rev. A15, 975.

Russell, W.E., Reddy, S.P., and Cho, C.W. 1974. J. Mol. Spectrosc. 52, 72.

Sen, A. 1978. M.Sc. thesis, Memorial University of Newfoundland (unpublished).

Sen, A., Prasad, R.D.G., and Reddy, S.P. 1980. J. Chem. Phys. 72, 1716.

Sinha, B.B.P. 1967. M.Sc. thesis, Memorial University of Newfoundland (unpublished).

Van Kranendonk, J. 1957. Physica 23, 825.

Van Kranendonk, J. 1958. Physica 24, 347.

Van Kranendonk, J. 1968. Can. J. Phys. 46, 1173.

Watanabe, A., and Welsh, H.L. 1965. Can. J. Phys. 43, 818.

Welsh, H.L. 1972. MTP International Review of Science, Physical Chemistry Vol. 3, Spectroscopy (Ed. D.A. Ramsay, Butterworths, London).

Woolley, H.W., Scott, R.B., and Brickwedde, F.G. 1948. J. Res. Natl. Bur. Standards 41, 396.